Global isotopic proxy records for Ordovician temperature reconstruction

Authors:

Xiaoli Ma[1,2], Yiying Deng[3], Linna Zhang[4], Terry Isson[5], Isabel P. Montañez[6,7], Junxuan Fan[1,2]

Affiliations:

[1]School of Earth Sciences and Engineering and Frontiers Science Center for Critical Earth Material Cycling, Nanjing University, Nanjing 210023, China

[2]State Key Laboratory of Critical Earth Material Cycling and Mineral Deposits, Nanjing University, Nanjing 210023, China

[3]School of Resources and Environmental Engineering, Hefei University of Technology, Hefei 230009, China

[4]Key Laboratory of Palaeobiology and Petroleum Stratigraphy, Nanjing Institute of Geology and Palaeontology, Chinese Academy of Sciences, Nanjing 210008, China

[5]Te Aka Mātuatua, University of Waikato (Tauranga), Bay of Plenty, Tauranga, New Zealand

[6]Department of Earth and Planetary Sciences, University of California, Davis, CA 95616, USA

[7]Institute of the Environment, University of California, Davis, CA 95616, USA

Correspondence: Isabel P. Montañez (ipmontanez@ucdavis.edu) and Junxuan Fan (jxfan@nju.edu.cn)

Preprint statement: This manuscript is a non-peer-reviewed preprint submitted to EarthArXiv and is currently under consideration for publication in *Earth System Science Data*.

Abstract

The Ordovician represents a critical interval in the Phanerozoic, marked by two profound biological events: the Great Ordovician Biodiversification Event (GOBE), with an unprecedented tenfold increase in marine species diversity, which was abruptly terminated by the Late Ordovician Mass Extinction (LOME), one of the most severe extinction events in Earth's history, wiping out approximately 85% of marine species. Paleotemperature reconstructions are crucial for understanding the Ordovician climate change. Here, we develop a transparent multi-criteria quality-control framework integrating stratigraphic, petrographic, sedimentological, and geochemical constraints to evaluate the preservation of individual isotopic proxy values. Applying this framework, we construct *OrdoTemp* that presents 5,223 high-quality isotopic proxy data, rigorously screened from 15,367 measurements. This dataset contains oxygen isotope ($\delta^{18}O$) data from carbonate bulk rock, brachiopod, and conodont fossils (98.5%), as well as carbonate clumped isotope (Δ_{47}) data (1.5%). This dataset can contribute to investigations of Ordovician climate change at regional or global scales, helping to understand Ordovician climate system change against the background of GOBE and LOME. The dataset is freely available at https://doi.org/10.5061/dryad.2jm63xt6h (Ma et al., 2026).

1 Introduction

The Ordovician Period (486.85 Ma to 443.1 Ma) marked a pivotal transition in Earth's history. It included the Great Ordovician Biodiversification Event (GOBE), when Family-, genus-, and species-level diversity increased strongly, and the Late Ordovician Mass Extinction (LOME), the first of five mass extinctions in the Phanerozoic, resulted in the elimination of approximately 50% of marine genera and 85% of marine species (Sepkoski, 1995; Harper et al., 2014; Alroy, 2010; Servais et al., 2016; Fan et al., 2020; Deng et al., 2021; Sheehan, 2001; Stanley, 2016; Kröger et al., 2019). These biological changes were closely related to climate and environmental change. Cooling, marine transgression, ocean oxygenation, glaciation, regression, and anoxia have all been proposed as important controls (Trotter et al., 2008; Servais et al., 2009; Edwards et al., 2017; Lindskog et al., 2023; Bond & Grasby, 2020; Bergmann et al., 2025; Liu et al., 2025).

Deep-time climate reconstructions are fairly challenging because all paleoclimate proxy records are influenced by factors other than climate. Of all geological periods of the Phanerozoic, reconstructing the Ordovician climate has attracted widespread attention. Previous studies have used oxygen isotopes ($\delta^{18}O$) and carbonate clumped isotopes (Δ_{47}) of fossil shells, such as brachiopods and conodonts, to estimate ancient seawater temperature (e.g. Shields et al., 2003; Trotter et al., 2008; Finnegan et al., 2011; Rasmussen et al., 2016; Bergmann et al., 2018; Jin et al., 2018; Wheeley et al., 2018; Barney and Grossman, 2022). These fossil archives can provide reliable records when they are well preserved, but suitable fossil material is not always common in Ordovician rocks. The $\delta^{18}O$ records from bulk carbonate rocks are more abundant and can fill the gap caused by the paucity of fossil materials (Goldberg et al., 2021), due to the large number of published data including the Precambrian and the Phanerozoic (Bergmann et al., 2022). However, they are more vulnerable to diagenetic alteration: cementation, recrystallisation, replacement, burial heating, and interaction with diagenetic fluids can partly or fully modify the original $\delta^{18}O$ signal (Brand and Veizer, 1980; Banner and Hanson, 1990; Quinn, 1991; Marshall, 1992; Swart, 2015; Jacobsen and Kaufman, 1999). In theory, if diagenetic stabilisation of carbonate host occurred under low water-rock ratios, then the original $\delta^{18}O$ signal can be minimally altered (Brand and Veizer, 1980; Banner and Hanson, 1990; Marshall, 1992; Jacobsen and Kaufman, 1999). Furthermore, the Δ_{47}-temperature, mineral $\delta^{18}O$ and calculated fluid $\delta^{18}O$ data of brachiopods and micrites revealed that primary $\delta^{18}O$ compositions could be largely (but not perfectly) preserved in closed diagenetic systems with low fluid availability, despite the resetting of carbonate clumped isotope temperatures (Bergmann et al., 2018; Goldberg et al., 2021; Thiagarajan et al., 2024). Therefore, it is essential to establish systematic screening methods for diagenetic alteration to identify these least altered bulk-rock $\delta^{18}O$ values for deep-time climate studies.

Here, we build the *OrdoTemp* database including 15,367 isotopic values from bulk carbonate rocks (12,171) and fossil shells. To improve the reuse of bulk-carbonate $\delta^{18}O$ records, we developed a transparent quality-control framework. The workflow evaluates age quality and petrographic and geochemical evidence for all $\delta^{18}O$ proxy data. For bulk-carbonate $\delta^{18}O$ records, it additionally assesses lithology, depositional setting, quantitative $\delta^{18}O$ patterns, and consistency with independent fossil-derived $\delta^{18}O$ records. After a series of quality-control criteria, 5,223 measurements (with 2,769 bulk-carbonate $\delta^{18}O$) were retained as better-preserved values, representing 34% of the original dataset. For each proxy value, we assigned numerical ages and calibrated them to the same stratigraphic framework: the Geological Time Scale 2020 (GTS 2020, Goldman et al., 2020).

This dataset can be used to understand the Ordovician climate system changes within the background of GOBE and LOME, for example, 1) uncover the temporal and spatial patterns of Ordovician climate change at a global scale; 2) assess regional climate change; 3) validate the results of climate model simulations; 4) explore links among climate, the GOBE, and the LOME. More importantly, 5) this dataset provides a quality-assessed framework to make bulk-carbonate $\delta^{18}O$ reusable for deep-time temperature reconstruction. Version 0.0.1 is available on Dryad (https://doi.org/10.5061/dryad.2jm63xt6h; Ma et al., 2026).

2 Data and methods

2.1 Data collection

The *OrdoTemp* database was compiled from 82 documents published between 1986 and 2026 (Table 1). These include 80 journal articles, one bachelor's thesis, and one conference paper. Bulk-carbonate $\delta^{18}O$ data were searched in Web of Science and Google Scholar as key words: Ordovician carbonate oxygen isotope. We screened about ~300 candidate documents and finally retained 45 studies that reported new bulk-carbonate $\delta^{18}O$ measurements (Table 1). Fossil $\delta^{18}O$ data, including brachiopod and conodont data, were first extracted from the PhanSST database (Judd et al., 2022). We then added Ordovician fossil records published between 2023 and March 2026, in total, giving 32 source documents for fossil $\delta^{18}O$ data (Table 1). Carbonate clumped-isotope data were collected using the same search and screening procedure, which identified five relevant documents (Table 1).

All values were compiled manually. For each sample, we collected the isotope value, sampling depth, lithology, biostratigraphy, depositional-environment setting, modern location, paleocontinent, and available supporting geochemical data, etc. Table and spreadsheet data were entered directly. However, a very small amount of data in PDF or Word files was converted to spreadsheet format, and values shown only in figures were digitised with WebPlotDigitizer-4.5 (Rohatgi, 2021).

In total, the database includes 222 sections or outcrops, showing a stratigraphic range from the Miaolingian (Cambrian) to the Llandovery (Silurian) (Table 1). These sections or outcrops were derived from the United States of America, China, Canada, Russia, Estonia, Sweden, Argentina and Norway. (Fig. 1). There are four proxy types: $\delta^{18}O_{bulk}$, $\delta^{18}O_{brach}$, and $\delta^{18}O_{cono}$, and Δ_{47}. $\delta^{18}O_{bulk}$, $\delta^{18}O_{brach}$, and $\delta^{18}O_{cono}$ refer to the $\delta^{18}O$ data obtained from bulk carbonate rocks, brachiopod fossils, and conodont fossils, representing 79.2%, 7.8% and 11.6% of the database, respectively. Δ_{47} refers to the carbonate clumped isotopes from micrites or brachiopod fossils, representing 1.4% of the database (Fig. 1).

Table 1. Summary of data sources represented in the *OrdoTemp* database.

Each data source corresponds to its reference label. The sampling site column lists unique section/core or outcrop names in each reference. The number of isotopic measurements equals the number of entries (rows). Stratigraphic range is summarised using only the oldest and youngest stratigraphic terms of the section/core or outcrop. Archive type lists the archive type of proxy data.

Data source	Sampling site	Number of isotopic measurements	Stratigraphic range	Archive type
Ainsaar et al., 1999	Pärnu–6; Ristiküla–174; Tartu–453	121	Sandbian—Katian	bulk-carbonate $\delta^{18}O$
Albanesi et al., 2020	Marathon; Saint Paul's Inlet; Western Brook Pond; Wilcox Pass; Precordillera	44	Stage 10—Hirnantian	conodont $\delta^{18}O$
Avila et al., 2022	I-35N	20	Dapingian—Sandbian	conodont $\delta^{18}O$
Azmy and Jin, 2019	Site 2; Site 3; Site 1	59	Sandbian—Hirnantian	brachiopod $\delta^{18}O$
Azmy et al., 2014	Green Point	84	Furongian—Floian	bulk-carbonate $\delta^{18}O$
Barney and Grossman, 2022	Jessamine Dome	52	middle Katian—late Katian	brachiopod $\delta^{18}O$; brachiopod Δ_{47}
Bartlett et al., 2018	Anticosti Island	8	Katian—Rhuddanian	conodont $\delta^{18}O$
Bassett et al., 2007	Lange Ranch	9	Tremadocian	conodont $\delta^{18}O$
Bergmann et al., 2018	Unknown	64	Guzhangian—Rhuddanian	brachiopod $\delta^{18}O$; brachiopod Δ_{47}
Brand, 2004	Maysvillian	3	Sandbian—Hirnantian	brachiopod $\delta^{18}O$
Brookfield and Hannigan, 2021	OGS 83-5	28	Katian	brachiopod $\delta^{18}O$
Buggisch et al., 2010	Frankfort East/64S2; Bear Creek/60BCK; Moffett Road/60BCK; Minnesota; Dead Horse Quarry	200	Sandbian—Katian	conodont $\delta^{18}O$
Calner et al., 2021	Bronnoya Pilbogen Bay; Bronnoya Store Ostsundet; Hovedoya; Konglungø; Olledalen Skytebane; Vettre	205	Katian—Rhuddanian	bulk-carbonate $\delta^{18}O$

Chen et al., 2022	Xilinggou; Zhaolaoyu	107	Darriwilian—Sandbian	bulk-carbonate $\delta^{18}O$
Dent et al., 2021	Olympic 1 well	44	Tremadocian—Dapingian	bulk-carbonate $\delta^{18}O$
Diamond, 2013	Meiklejohn Peak	81	Darriwilian—Sandbian	bulk-carbonate $\delta^{18}O$
Edward et al., 2022	Degerhamn Quarry; Horns Udde North; Horns Udde South; Kårehamn; Kårehamn P4	342	Floian—Sandbian	bulk-carbonate $\delta^{18}O$; brachiopod $\delta^{18}O$
Edwards and Saltzman, 2014	Ibex; Shingle Pass	470	Furongian—Darriwilian	bulk-carbonate $\delta^{18}O$
Edwards and Saltzman, 2016	Bally Mountain and Interstate–35; Clear Spring; Ibex; Meiklejohn Peak	838	Tremadocian—Darriwilian	bulk-carbonate $\delta^{18}O$
Edwards et al., 2021	63AB; 75HB; 75HA; Hill 8308; Arbuckle Mountains; Shingle Pass	108	Tremadocian—Katian	conodont $\delta^{18}O$
Elrick et al., 2013	Kentucky; Anticosti Island	62	Katian	conodont $\delta^{18}O$
Fan et al., 2015	Liangcun; Shatan; Xiaogangwan; Zhuazhuayan	102	Darriwilian—Katian	bulk-carbonate $\delta^{18}O$
Finnegan et al., 2011	Anticosti Island; OH/KY; SE Minnesota	49	Katian—Hirnantian	brachiopod $\delta^{18}O$; brachiopod Δ_{47}
Goldberg et al. 2021	Ny Friesland; Port au Port Peninsula; Unknown	128	Wuliuan—Sheinwoodian	bulk-carbonate $\delta^{18}O$; brachiopod $\delta^{18}O$; brachiopod Δ_{47}
Gong et al., 2021	Daling; Dingxiang	223	Darriwilian—Sandbian	bulk-carbonate $\delta^{18}O$
Henderson et al., 2018	Las Aguaditas Creek; Las Chacritas River	222	Darriwilian—Sandbian	bulk-carbonate $\delta^{18}O$
Herrmann et al., 2010	Sogn	71	Sandbian—Katian	conodont $\delta^{18}O$

Hu et al., 2021	Dingjiawan; Huanghuachang; Lianghekou	197	Tremadocian—Dapingian	bulk-carbonate $\delta^{18}O$
Husinec and Leslie, 2022	Beaver Lodge–Ordovician Unit 1; Berg 15–24; BLSUE–406; Church 1–2; Simpson 1–H	265	Katian—Telychian	bulk-carbonate $\delta^{18}O$
Jin et al., 2018	Gukongkou; Jieling; Hengdu; Kuanyinqiao	33	Tremadocian—Hirnantian	conodont $\delta^{18}O$
Jones et al., 2016	Barn Hills; Monitor Range; Pancake Range; Silver Island NE; Silver Island NW; South Egan Range	776	Katian—Rhuddanian	bulk-carbonate $\delta^{18}O$
Jones et al., 2011	911; 914; 920; D801–6, 901; D804, 901; D814, 909A/B; D815, 912, 912A; D816, D817; D821	466	Katian—Rhuddanian	bulk-carbonate $\delta^{18}O$
Kaljo et al., 2004	Kaugatuma; Kõrgessaare; Orjaku; Rapla; Saku 1098A; Vasalemma 772; Viljandi	386	Sandbian—Llandovery	bulk-carbonate $\delta^{18}O$
Kaljo et al., 2007	Kerguta 565; Mehikoorma 421; Valga 10	326	Dapingian—Hirnantian	bulk-carbonate $\delta^{18}O$
Kouchinsky et al., 2008	Kulyumbe River	1118	Drumian—Tremadocian	bulk-carbonate $\delta^{18}O$
Kump et al., 1999	Copenhagen Canyon	47	Katian—Rhuddanian	bulk-carbonate $\delta^{18}O$
LaPorte et al., 2009	Blackstone River; Monitor Range; Vinini Creek	287	Katian—Hirnantian	bulk-carbonate $\delta^{18}O$
Li et al., 2018	Qiliao	47	Tremadocian—Hirnantian	bulk-carbonate $\delta^{18}O$
Liu et al., 2016	S112–1; S114	84	Darriwilian—Katian	bulk-carbonate $\delta^{18}O$
Liu et al., 2022a	Kalpin Shuinichang; Dawangou	99	Tremadocian—Katian	conodont $\delta^{18}O$

Liu et al., 2022	Wuke	69	Katian—Llandovery	bulk-carbonate $\delta^{18}O$
Ma et al., 2015	Jieling; Puxihe; Zhenjin	69	Darriwilian—Katian	bulk-carbonate $\delta^{18}O$
Männik et al., 2021	Mehikoorma 421; Valga 10	92	Darriwilian—Hirnantian	conodont $\delta^{18}O$
Mauviel et al., 2020	Anticosti Island	510	Katian—Rhuddanian	bulk-carbonate $\delta^{18}O$
McLaughlin et al., 2016	NACP core	441	Floian—Rhuddanian	bulk-carbonate $\delta^{18}O$
Metzger and Fike, 2013	Highway MM; New London	114	Floian—Rhuddanian	bulk-carbonate $\delta^{18}O$
Middleton et al., 1991	Unknown	42	Sandbian—Hirnantian	brachiopod $\delta^{18}O$
Munnecke et al., 2011	Daijiagou; Dajiaosi; Hengdu quarry; Hengtang quarry; Honghuayuan; Huangnitang; Liujia; Putangkou; Sanqushan; Yanmen Power Station Quarry; Zhuzhai	489	Tremadocian—Rhuddanian	bulk-carbonate $\delta^{18}O$
Qing and Veizer, 1994	Anticosti Island; Unknown	102	Tremadocian—Hirnantian	brachiopod $\delta^{18}O$
Quinton and MacLeod, 2014	60BCK; 75HA; 75HB; 75HC; 63AA; 64AB	131	middle Katian—late Katian	conodont $\delta^{18}O$
Quinton et al., 2016	Fort Payne; Gadsden; Red Mountain Expressway; Tidwell Hollow	324	Sandbian—Katian	bulk-carbonate $\delta^{18}O$
Quinton et al., 2017	Decorah; Dickeyville; Hagen; Red Mountain; Rochester; Tidwell Hollow	265	Sandbian—Katian	conodont $\delta^{18}O$
Quinton et al., 2021	Union Furnace	177	Sandbian	bulk-carbonate $\delta^{18}O$
Quinton et al., 2018	Lange Ranch	98	Tremadocian	conodont $\delta^{18}O$

Rasmussen et al., 2016	Lynna River Valley; Putilovo Quarry	352	Floian—Darriwilian	brachiopod $\delta^{18}O$
Rosenau et al., 2012	Fittstown	53	Sandbian—Katian	conodont $\delta^{18}O$
Saltzman and Young, 2005	Monitor Range–Antelope Range Composite	141	Dapingian—Katian	bulk-carbonate $\delta^{18}O$
Shields et al., 2003	Anticosti Island; Unknown; Amadeus Basin; Utah; St. Petersburg; Arbuckle Mountains; Cincinnati; St. Louis; Lexington	181	Tremadocian—Rhuddanian	brachiopod $\delta^{18}O$
Sial et al., 2013	Cerro La Chilca; Las Aguaditas; Quebrada Juan Pobre	168	Drumian—Sandbian	bulk-carbonate $\delta^{18}O$
Thiagarajan et al., 2024	Unknown	154	Dapingian—Rhuddanian	brachiopod $\delta^{18}O$; bulk-carbonate $\delta^{18}O$; brachiopod Δ_{47}
Thompson and Kah, 2012	Cerro La Silla; Table Point	161	Floian—Darriwilian	bulk-carbonate $\delta^{18}O$
Trela et al., 2022	Mojcza	121	Katian—Hirnantian	conodont $\delta^{18}O$
Trotter et al., 2008	Devon Island; Manitoba; Tempe Downs; Anticosti Island; Black Mountain; Saint Paul's Inlet; Western Brook Pond; Emanuel Creek	20	Tremadocian—Sheinwoodian	conodont $\delta^{18}O$
Veizer et al., 1999	Anticosti Island	5	Hirnantian	brachiopod $\delta^{18}O$
Veizer et al., 1986	Anticosti Island	24	Hirnantian	brachiopod $\delta^{18}O$
Wadleigh and Veizer, 1992	Unknown	90	Tremadocian—Hirnantian	brachiopod $\delta^{18}O$
Wheeley et al., 2018	Cow Head Peninsula	32	Tremadocian—Floian	conodont $\delta^{18}O$

Wheeley et al., 2012	Unknown	40	Tremadocian—Hirnantian	conodont $\delta^{18}O$
Wu et al., 2017	Tingskullen	313	Floian—Darriwilian	bulk-carbonate $\delta^{18}O$
Wu et al., 2018	Killeröd Quarry	90	Darriwilian	bulk-carbonate $\delta^{18}O$
Wu et al., 2020	Daling; Gukongkou; Xiangshuidong	540	Tremadocian—Darriwilian	bulk-carbonate $\delta^{18}O$
Xie et al., 2019	Houtan; Yangjiaping	202	Furongian—Hirnantian	bulk-carbonate $\delta^{18}O$
Yang et al., 2021	Dabantage; Shuinichang; Tabei Wells; Yingshanbeipo	199	Furongian—Darriwilian	bulk-carbonate $\delta^{18}O$
Young et al., 2016	Arbuckle Mountains; Clear Spring	155	Darriwilian—Sandbian	bulk-carbonate $\delta^{18}O$
Young et al., 2005	Boonsborough, Frankfort and Minerve; Dolly Ridge; Fittstown; Hagan	270	Sandbian—Katian	bulk-carbonate $\delta^{18}O$
Young et al., 2010	Kardla; Western Anticosti Island Composite	219	Katian—Rhuddanian	bulk-carbonate $\delta^{18}O$
Yu et al., 2019	Jiacun	28	Darriwilian	bulk-carbonate $\delta^{18}O$
Zaitsev and Pokrovsky, 2014	Babino quarry; Lynna River	91	Floian—Darriwilian	bulk-carbonate $\delta^{18}O$
Zhang et al., 2010	Honghuayuan	63	Tremadocian—Hirnantian	bulk-carbonate $\delta^{18}O$
Zhang and Munnecke, 2016	Dabantag No.2; Dabantag No.3; Dawangou; Queerqueke Mountains; Sishichang; Tazhong–4; Uligezhitag; Yaerdang; Yangjikan	582	Tremadocian—Katian	bulk-carbonate $\delta^{18}O$
Zhang et al., 2026	Hällekis; Kinnekulle -1 core	105	Floian—Katian	conodont $\delta^{18}O$
Zhao et al., 2025	Huanghuachang-Chenjiahe-Wangjiawan Composite	170	Tremadocian—Rhuddanian	conodont $\delta^{18}O$

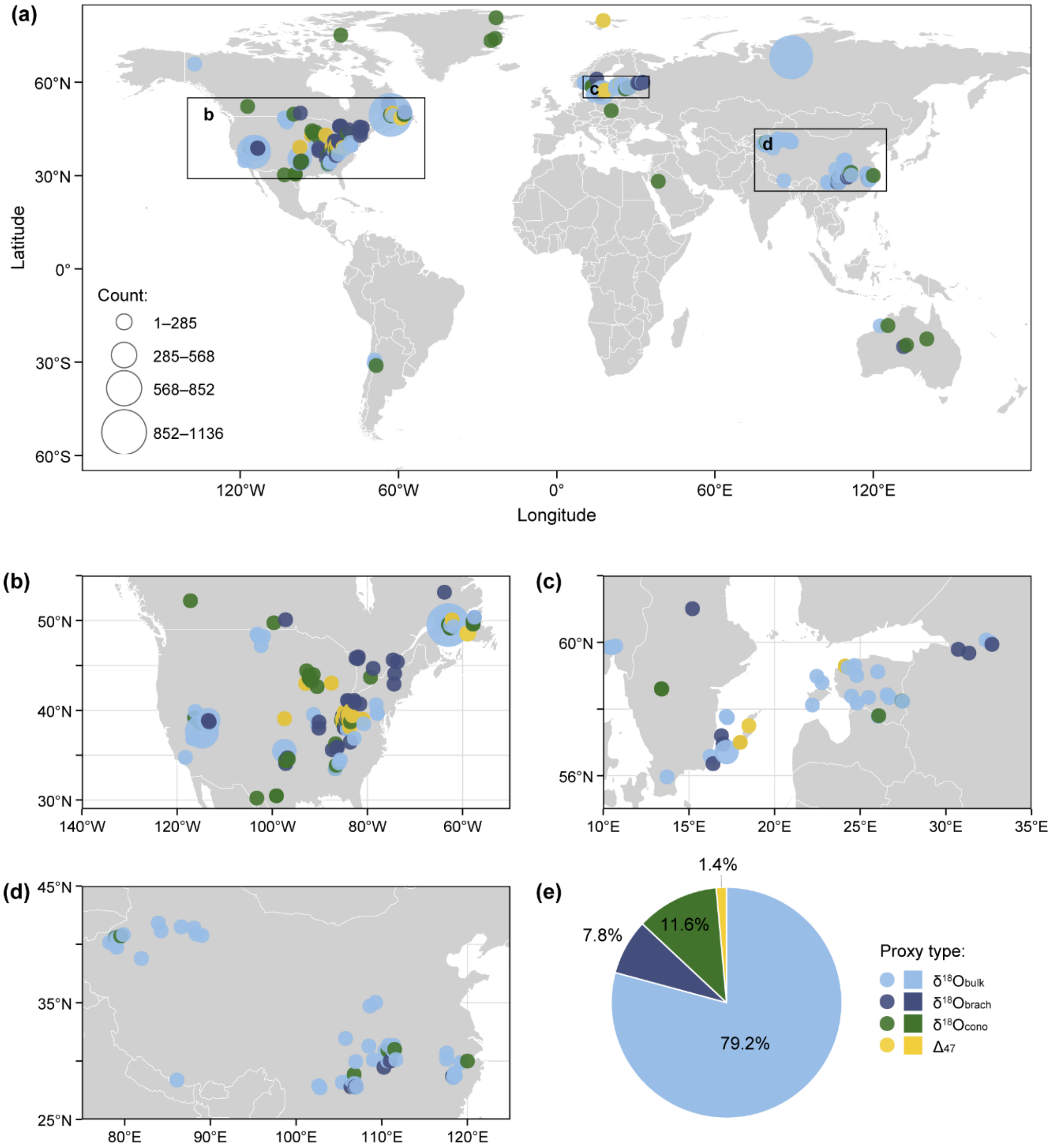

Figure 1. Modern geographic distribution and proxy composition of the *OrdoTemp* database. (a) Global sampling locations. Symbol colour denotes proxy type, and symbol size denotes the number of isotopic measurements. Boxes mark the enlarged regions shown in **(b)** Laurentia, **(c)** Baltoscandia, and **(d)** China and adjacent areas. **(e)** Proportion of the proxy types.

2.2 Conodont $\delta^{18}O$ standardisation and correction

The $\delta^{18}O$ values from bulk carbonates and brachiopod fossils were kept as reported in the original studies. For the Δ_{47} values, although laboratory-specific Δ_{47}–temperature calibrations are internally reliable, interlaboratory differences in Δ_{47} data correction raise concerns about the direct comparability of these Δ_{47} values (Bernasconi et al., 2021). Thus, no additional corrections were applied to the published Δ_{47} values. However, the $\delta^{18}O$ data of conodont fossils were compiled from studies that used different reference standards and analytical methods. Note that some $\delta^{18}O_{cono}$ data in our database, compiled from the PhanSST database (Judd et al., 2022), were provided by Grossman and Joachimski (2020), and these are the uncorrected published values. Therefore, for all $\delta^{18}O_{cono}$ data, we applied a common correction workflow. Firstly, all $\delta^{18}O_{cono}$ data were normalised to the same reference standard (NBS120c=21.7‰; Lécuyer et al., 2013). Secondly, we corrected for analytical bias related to different measurement techniques. In situ secondary ion mass spectrometry (SIMS) measurements of $\delta^{18}O$ are systematically higher than conventional thermally coupled elemental analyser-isotope ratio mass spectrometry (TC-EA IRMS) measurements by ~0.6–1.3‰, as determined by analysing modern marine bioapatite and extinct conodonts (Trotter et al., 2015). Here, the SIMS-measured $\delta^{18}O_{cono}$ data were adjusted by 0.6‰ (Trotter et al., 2016) to align with the IRMS-measured records. Finally, we stored the originally reported value in the field *proxyValue* and the corrected value in the field *correctedProxyValue* (Ma et al., 2026).

2.3 Age constraint

We assigned numerical ages using the stratigraphic information available for each measurement (Fig. 2a). All ages were calibrated to the GTS 2020 (Goldman et al., 2020). The biostratigraphic information was first used where standard biozones (such as conodonts, chitinozoans, graptolites or trilobites) were available. Specifically, the lower and upper boundaries of the standard biozone are set as age anchors, and the sediments between the two boundaries are assumed to have a constant sedimentation rate. If biostratigraphic subdivisions are not available, chronostratigraphy (at the stage or substage level) is used instead. Another situation arises when biostratigraphic information only provides a broad age estimate; then the chemostratigraphic information is used to refine it. For example, the proxy value's numerical age from the Copenhagen Canyon section (Nevada) was assigned by both biostratigraphy and chemostratigraphy (Kump et al., 1999). Using an approach proposed by Pulsipher et al. (2021), we identified the pre-, peak and post-peak stages of well-defined carbon isotope excursions, such as the Hirnantian Carbon Isotope Excursion (Cramer and Jarvis, 2020). We then used these to constrain the data age more precisely. Additionally, there is very little radioisotopic data (based on the CA-IDTIMS dates of bentonite beds) available, which can be used to constrain the data ages (e.g., the Olympic 1 well in Dent et al., 2021).

Note that some fossil-derived $\delta^{18}O$ data extracted from PhanSST, that have primarily been constrained to the stage level (see Judd et al., 2022), and that all biostratigraphic information and absolute ages are relative to GTS 2020 provided from the StabisoDB (Grossman and Joachimski, 2020). Here, we manually searched for related stratigraphic study references to attempt to calibrate all these $\delta^{18}O$ data ages to higher temporal resolution stratigraphic frameworks, such as standard biozonations. For some proxy data, we can only follow numerical ages provided in the primary articles due to a lack of further stratigraphic information (see Finnegan et al., 2011; Bergmann et al., 2018; Goldberg et al., 2021; Barney and Grossman, 2022; Thiagarajan et al., 2024).

We then graded the age constraint quality according to the uncertainty of the biostratigraphic and chronostratigraphic information (see Fig. 2b). If the lower and upper boundaries of a biozone or stage were certain, the age constraint quality was categorised as 'excellent'. Otherwise, we calculated the age confidence interval for each data point, defined as the age difference between the nearest certain lower or upper boundary of a biozone or stage containing the data point. There is an exception: if there was any disconformity or hiatus within or across the biozone or stage, which spans a relatively long duration (e.g., > 1 Myr), all data points from that interval were directly considered as poorly constrained. Therefore, it was unnecessary to calculate their age confidence interval. We then introduced the age confidence ratio for well-constrained data points, defined as the age confidence interval divided by the stage duration, to evaluate whether the age confidence interval exceeds the stage duration. According to these values, we categorised the data into three additional groups: 'good', 'moderate', and 'poor', with ratios of 0–0.1, 0.1–1, and > 1, respectively. However, some proxy data could not be assigned an age quality due to insufficient stratigraphic information, marked as 'unknown'.

In total, 90.8% of isotopic proxy data (13,957) can be assigned a numeric age through various age constraint reference information in the articles (Fig. 2a). The remaining 9.2% (1,410 values; marked as 'not available' in Fig. 2a) cannot be calibrated. Most ages are based on biostratigraphy (46.2%) or chronostratigraphy (36.7%). Smaller proportions use chemostratigraphy (2.9%), combined methods (3.2%), primary-source information (1.8%), or rare radioisotopic dates (0.1%). Among them, age-quality classes are dominated by excellent (42.3%) and moderate (41.5%) measurements, with smaller proportions of good (1.4%), poor (3.8%), and unknown (1.8%) (Fig. 2b).

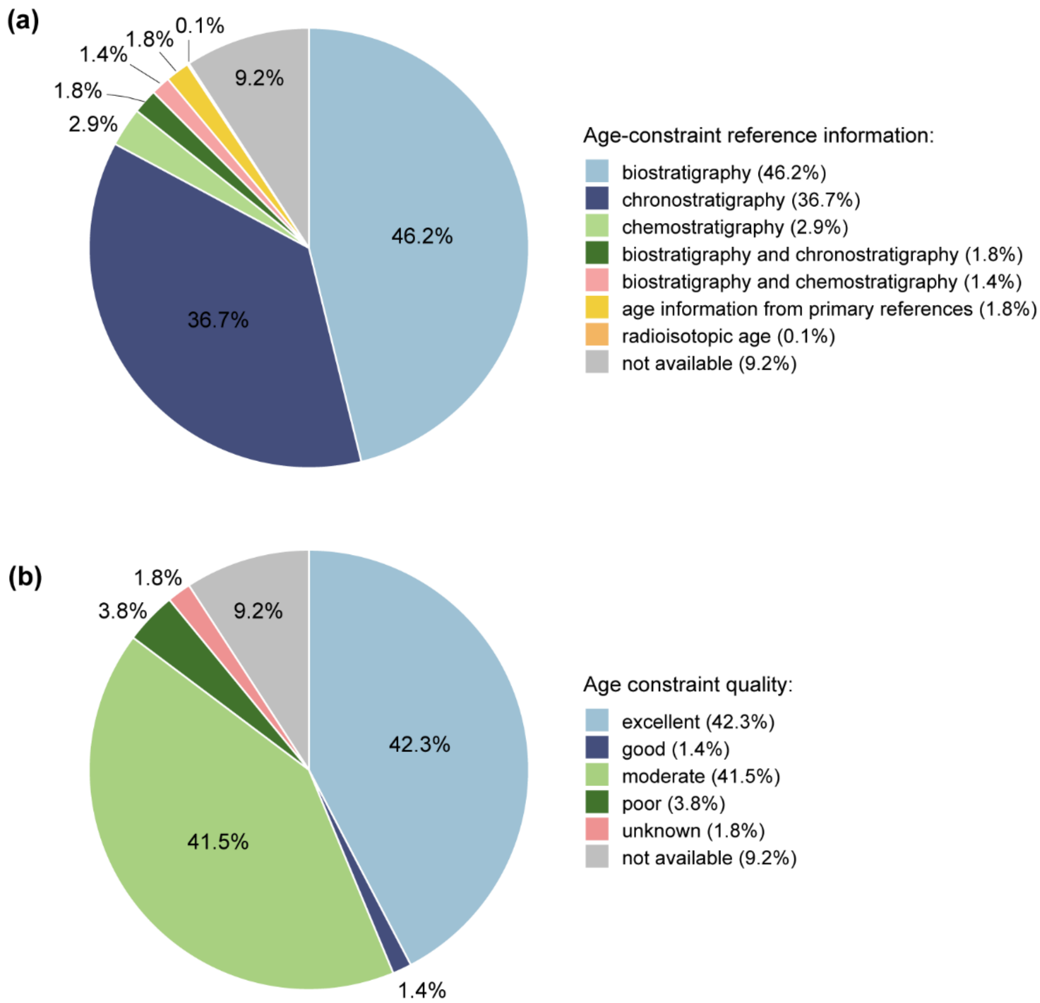

Figure 2. Age constraint metadata in the *OrdoTemp* database. (a) Age-constraint reference information. **(b)** Assigned age-constraint quality. Percentages are calculated relative to the complete database, including the 1,410 measurements (9.2%) for which a numerical age is not available.

2.4 Quality control

2.4.1 Age screening

Age screening improved the age constraint quality of the database. We kept proxy values with \`excellent\`, \`good\`, or \`moderate\` age quality, because these proxy values have acceptable age uncertainty with age confidence ratio <1. The data labelled ‘unknown’ were pended. By contrast, proxy values labelled \`poor\` or \`not available\` were removed from the dataset. These measurements either have large age uncertainty with age confidence ratio >1, or limited stratigraphic information, or cannot be able to assign numerical age (see details in 2.3 Age constraint).

It is worth noting that some measurements that we removed come from intervals with unconformities or hiatuses, which make age interpolation unreliable. It is possible that these unconformities/hiatuses resulted from sea-level fall, when shallow-water carbonates may be exposed to meteoric fluids, and thus modify the original isotope signal (Banner and Hanson, 1990; Marshall, 1992; Knauth and Kennedy, 2009). Thus, the age screening step not only removed poorly dated measurements but also some measurements with a higher risk of exposure-related alteration.

2.4.2 Lithology and depositional-environment screening

This screening step was aimed at keeping comparable calcite-dominated marine carbonate samples and removing measurements with a high risk of secondary or mixed isotope signals. Our compiled Ordovician $\delta^{18}O_{bulk}$ data were acquired from various lithological components, including limestones, dolostones, shales, sandstones, spars, and calcite veins. Firstly, we retained $\delta^{18}O_{bulk}$ data sampled from limestones or limestone-dominated rocks, e.g., where dolomite accounted for less than 5% of the rock components. These data were measured from bulk components that were sampled as far as possible from areas of strong weathering, altered material or secondary diagenetic veins. Herein, some were measured from fine-grained micritic components, such as micrites (lime mudstones) or the micritic matrix of wackestones or packstones. The micritic and fine-grained microsparitic fabrics, ooids, or small-scale sedimentary structures are included in primary depositional components which show recrystallisation that often occurred during sedimentation or shallow burial, and have high potential to contain compositions similar to primary seawater (Kaufman et al., 1991; Kaufman and Knoll, 1995; Frank et al., 1997; Horacek et al., 2010; Kah et al., 2012; Gilleaudeau et al., 2018).

By contrast, the $\delta^{18}O_{bulk}$ samples including sparry calcite, fracture-filling calcite, carbonate cements, and carbonate phases hosted in sandstone- or shale-dominated rocks were also excluded. These materials may represent secondary diagenetic components resulting from later fluid flow, cementation, recrystallisation, or burial reactions (Banner and Hanson, 1990; Marshall, 1992; Kah et al., 1999; Swart, 2015; Montañez and Crossey, 2018). We also excluded the $\delta^{18}O_{bulk}$ data from dolostones or dolostone-dominated rocks because dolomites can form or recrystallise during different diagenetic stages and may record $\delta^{18}O$ values different from coexisting calcite (Warren, 2000; Gregg et al., 2015; Petrash et al., 2017).

Additionally, we also used the depositional-environment attributes of proxy data to help screen out proxy data remarkably impacted by regional perturbations. Specifically, the data reported from exposure, strong restriction, or non-marine depositional environments in the original studies were excluded. These settings can be strongly affected by evaporation, freshwater input, and/or limited exchange with the open ocean, thus recording local isotopic signals (Banner and Hanson, 1990; Marshall, 1992; Knauth and Kennedy, 2009; Swart, 2015).

2.4.3 Published petrographic and geochemical screening

This screening step used diagenetic assessments based on petrographic and geochemical evidence reported in the source studies to further screen data. Petrographic observations include visual and optical inspections, microstructural examinations, or cathodoluminescence examinations to investigate the petrographic textures and fabrics of carbonate rocks, and thus to assess whether a sample preserved primary depositional fabrics or contained later diagenetic components (Kaufman et al., 1991; Marshall, 1992; Banner and Kaufman, 1994; McArthur, 1994; Brand et al., 2011). Geochemical indicators were also used as supporting evidence for diagenetic alterations, such as Mn, Fe, Sr and Mg, the $^{87}Sr/^{86}Sr$ ratios, as well as the $\delta^{13}C$-$\delta^{18}O$ covariation (Brand and Veizer, 1980; Veizer et al., 1992a; Veizer et al., 1992b; Denison et al., 1994; Banner, 1995; Brand et al., 2012; Garbelli et al., 2012). Since geochemical alterations during water-rock interaction exhibit predictable characteristics, analysing these compositions or ratios can help distinguish between well-preserved (least altered) and diagenetically altered carbonate rocks (Brand and Veizer, 1980; Banner and Hanson, 1990; Marshall, 1992; Denison et al., 1994). For example, Mn/Sr and Fe/Sr were expected to be higher in diagenetically altered carbonate rocks (Brand and Veizer, 1980; Banner and Hanson, 1990; Marshall, 1992; Kaufman and Knoll, 1995). The $^{87}Sr/^{86}Sr$ ratios could also reflect diagenetic alteration because post-depositional recrystallisation generally leads to an increase in $^{87}Sr/^{86}Sr$ ratios by incorporating ^{87}Sr that was released from evolved K-bearing silicates (rich in ^{87}Rb and thus higher $^{87}Sr/^{86}Sr$) into carbonate rocks (Gorokhov et al., 1995; Ovchinnikova et al., 1995; Fairchild et al., 2018). Therefore, the least altered carbonate rocks typically exhibit lower $^{87}Sr/^{86}Sr$ ratios (Shields and Veizer, 2002; Shields et al., 2003; Chen et al., 2022b). The co-variation between $\delta^{13}C$ and $\delta^{18}O$ is often cited as evidence of diagenetic alteration in a near-surface meteoric diagenetic environment due to the introduction of depleted ^{18}O and depleted ^{13}C from the subaerial recharge area (Brand and Veizer, 1980; Allan and Matthews, 1982; Banner, 1995; Knauth and Kennedy, 2009).

We examined and referred to the diagenetic assessment results in these original publications, and removed those $\delta^{18}O$ data that were expected to have been diagenetically altered. Specifically, measurements described as altered, recrystallised, veined, cemented, or geochemically unreliable were removed. For example, the published $\delta^{18}O_{bulk}$ data from the Aguathuna Formation at Table Point, western Newfoundland, were not included in this dataset because Thompson and Kah (2012) suggested this interval has experienced substantially greater postdepositional alteration. The published $\delta^{18}O_{bulk}$ data from the upper West Spring Creek Formation at Bally Mountain and Interstate-35, Oklahoma, were excluded because this interval could be the zone of meteoric diagenesis (Edwards and Saltzman, 2016).

2.4.4 Quantitative screening

Post-depositional diagenetic alteration generally lowers the $\delta^{18}O$ values of carbonate rocks in the near-surface meteoric diagenesis due to the introduction of ^{16}O in meteoric water, or in the deep-burial diagenesis because of increased burial temperatures (Veizer, 1983; Banner and Hanson, 1990; Quinn, 1991; Marshall, 1992; Knauth and Kennedy, 2009; Swart, 2015). Thus, higher $\delta^{18}O$ values in coeval material from marine sediments potentially represent primary signals of the ocean (Banner and Hanson, 1990; Marshall, 1992; Knauth and Kennedy, 2009; Brand et al., 2012; Swart, 2015; Rasmussen et al., 2016). Petrographic and geochemical screening supported this inference: well-preserved samples commonly plot in the more positive parts of $\delta^{18}O$–depth profiles, whereas altered samples tend to show lower values (Brand, 2004; Brand et al., 2012; Rasmussen et al., 2016).

Based on the above principles, we developed a quantitative approach to further screen the $\delta^{18}O_{bulk}$ data, while minimising the influence of outliers. We first used well-screened carbonate $\delta^{18}O$ data of brachiopod shells from the Ordovician Baltica section (Fig. S1a; Rasmussen et al., 2016) to identify the threshold value for this approach. These samples of the $\delta^{18}O_{brach}$ data were diagenetically photographed under SEM and assessed using Mn/Ca, Mg/Ca and Sr/Ca ratios for their preservational state (Rasmussen et al., 2016). The 352 $\delta^{18}O_{brach}$ data were divided into 17 depth bins, each containing ~20 data points. For each bin, we calculated the 1st to 100th percentiles of the $\delta^{18}O_{brach}$ data within the bin. We ignored the 1st percentile as it may contain abnormal negative $\delta^{18}O$ values, and calculated the 2nd–100th percentile range of $\delta^{18}O$ values, which is defined as the absolute difference between the 2nd and the 100th percentiles of the $\delta^{18}O$ values, to capture the well-preserved $\delta^{18}O_{brach}$ variability within each depth bin. We tested four candidate thresholds for this range: 0.8‰, 0.6‰, 0.4‰, 0.2‰. Values within the more positive window were classified as good (Fig. S1b-S1e). We then compared the results with those identified by Rasmussen et al. (2016) through petrographic and geochemical examination. The results revealed that setting the threshold at 0.8‰ would retain 95% of the good $\delta^{18}O_{brach}$ data identified by Rasmussen et al. (2016) (Fig. S1a-S1b). By contrast, applying values of 0.6‰, 0.4‰, or 0.2‰ would retain only 83%, 57% or 25% of the good $\delta^{18}O_{brach}$ data, respectively (Fig. S1c-S1e). Furthermore, only values of 0.8‰ and 0.6‰ can ensure significant consistency between the screened good data and that identified by Rasmussen et al. (2016).

Since the $\delta^{18}O$ data of Rasmussen et al. (2016) came from brachiopod shells, we then used Cenozoic deep-sea carbonate bulk-rock $\delta^{18}O$ data from ODP 1263 (Westerhold et al., 2020) to further evaluate whether the 0.8‰ 2^{nd}–100^{th} percentile range could reasonably represent the variability of well-preserved $\delta^{18}O$ data of bulk carbonates. The $\delta^{18}O_{bulk}$ data exhibited concentrated distributions and regular trends similar to those observed in benthic foraminifera, suggesting high data quality (see Fig. S2A in Westerhold et al., 2020). The 3,348 $\delta^{18}O_{bulk}$ data were divided into 149 depth bins. The 0.8‰ 2^{nd}–100^{th} percentile ranges of the $\delta^{18}O$ values showed a highly similar pattern to that of the original data (Fig. S2). Therefore, we selected 0.8‰ as the threshold to quantitatively screen the Ordovician $\delta^{18}O_{bulk}$ data in our dataset.

The Ordovician $\delta^{18}O_{bulk}$ data were derived from 142 sections/cores. The $\delta^{18}O_{bulk}$ data of each section/core were sorted into multiple bins according to their depth. To ensure that there are sufficient data points to observe the within-bin $\delta^{18}O_{bulk}$ variability, each depth bin was designed to contain ~20 data points. First, of the 625 depth bins in the 142 sections/cores, data points falling within the first percentile were excluded as they represented highly abnormal, negative outliers. Second, the more negative $\delta^{18}O_{bulk}$ data points within the 2^{nd} to 100^{th} percentiles but exceeding the 0.8‰ mean range were further excluded (see the four examples in Fig. S3). In this step, we only retained the more positive $\delta^{18}O_{bulk}$ data points that fell within the 0.8‰ mean range in each bin.

2.4.5 Consistency screening

The archives of brachiopod and conodont fossils consist of biogenic low-Mg calcite and carbonate-fluorapatite, respectively (Al-Aasm and Veizer, 1982; Sweet, 1989). Their mineral components are relatively resistant to diagenetic alteration (Al-Aasm and Veizer, 1982), with the latter considered to be more resistant than the former (Joachimski et al., 2004; Joachimski et al., 2009). Thus, the diagenetic potential of brachiopods and conodonts is relatively lower than that of bulk carbonates (Batt et al. 2007; Brand et al. 2012). To screen whether the bulk-carbonate $\delta^{18}O$ series preserve the same broad low-frequency signal as from independent biogenic archives (Fig. 3a and 3b), we compared the consistency among these different types of data ($\delta^{18}O_{bulk}$, $\delta^{18}O_{brach}$, $\delta^{18}O_{cono}$) in each paleogeographic region (Fig. 3 and Figs. S4). The screening step is based on this principle: if a bulk-carbonate series records a broad climate–ocean signal, it should vary in the same direction as independent fossil-derived $\delta^{18}O$ series from the same paleocontinent where temporal overlap is sufficient (Fig. 3c). Where different paleocontinents overlap in time, series from the same proxy type should also show broadly consistent trends (Fig. 3d–3f). It should also explain that this step does not require identical $\delta^{18}O$ values among all paleocontinents. It mainly focuses on shared long-term trends, because regional ocean circulation, water-mass structure, basin restriction, paleolatitudinal drift, and/or proxy-specific fractionation can produce real differences among regions (Männik et al., 2025). However, this approach still enables us to further screen out and exclude any $\delta^{18}O_{bulk}$ data that are inconsistent with the low-frequency signals of other data types.

We used the Spearman correlation results under 1-myr time bins, shown in Fig. 3. Within paleocontinents, Baltica and Laurentia show positive correlations among bulk-carbonate, brachiopod, and conodont $\delta^{18}O$ series (Fig. 3c). Baltica shows strong and significant cross-proxy agreement, with coefficients of 0.78 for bulk carbonate versus conodont, 0.76 for bulk carbonate versus brachiopod, and 0.75 for brachiopod versus conodont (Fig. 3c). Laurentia also shows positive cross-proxy correlations, with coefficients of 0.74 for bulk carbonate versus conodont, 0.70 for bulk carbonate versus brachiopod, and 0.52 for brachiopod versus conodont (Fig. 3c). Cross-paleocontinent comparisons further support the bulk-carbonate series (Fig. 3d). Bulk-carbonate series from Argentine Precordillera, Baltica, Laurentia, and Tarim show positive correlations with at least one better-supported regional bulk-carbonate series, with significant coefficients ranging from 0.57 to 0.85 (Fig. 3d).

South China is the main exception. Its bulk-carbonate $\delta^{18}O$ series is negatively correlated with the conodont series, with a coefficient of -0.68 (Fig. 3c). In contrast, the South China conodont series is positively correlated with conodont series from Baltica, Gondwana, Laurentia, and Tarim, with coefficients of 0.69, 0.63, 0.84, and 0.60, respectively (Fig. 3f). This pattern indicates that the conodont signal is consistent with the broader biogenic framework, but the South China bulk-carbonate series does not follow it. Additionally, cross-paleocontinent comparisons show the same result, with South China bulk carbonate negatively correlated with Argentine Precordillera and Laurentia, with coefficients of -0.61 and -0.56, respectively (Fig. 3d).

Based on these results, bulk-carbonate measurements from Argentine Precordillera, Baltica, Laurentia, and Tarim were retained (Fig. 3c and 3d). South China bulk-carbonate measurements younger than about 471 Ma were removed because they diverge from the conodont reference signal (Fig. 3c and 3f; Figs. S4). Older South China bulk-carbonate measurements were assigned to pending because they do not provide enough positive support for retention (Figs. S4). Besides, Gondwana and Siberia bulk-carbonate measurements were classified as pending because temporal overlap with independent archives is too limited for a secure decision (Fig. 3b–3d).

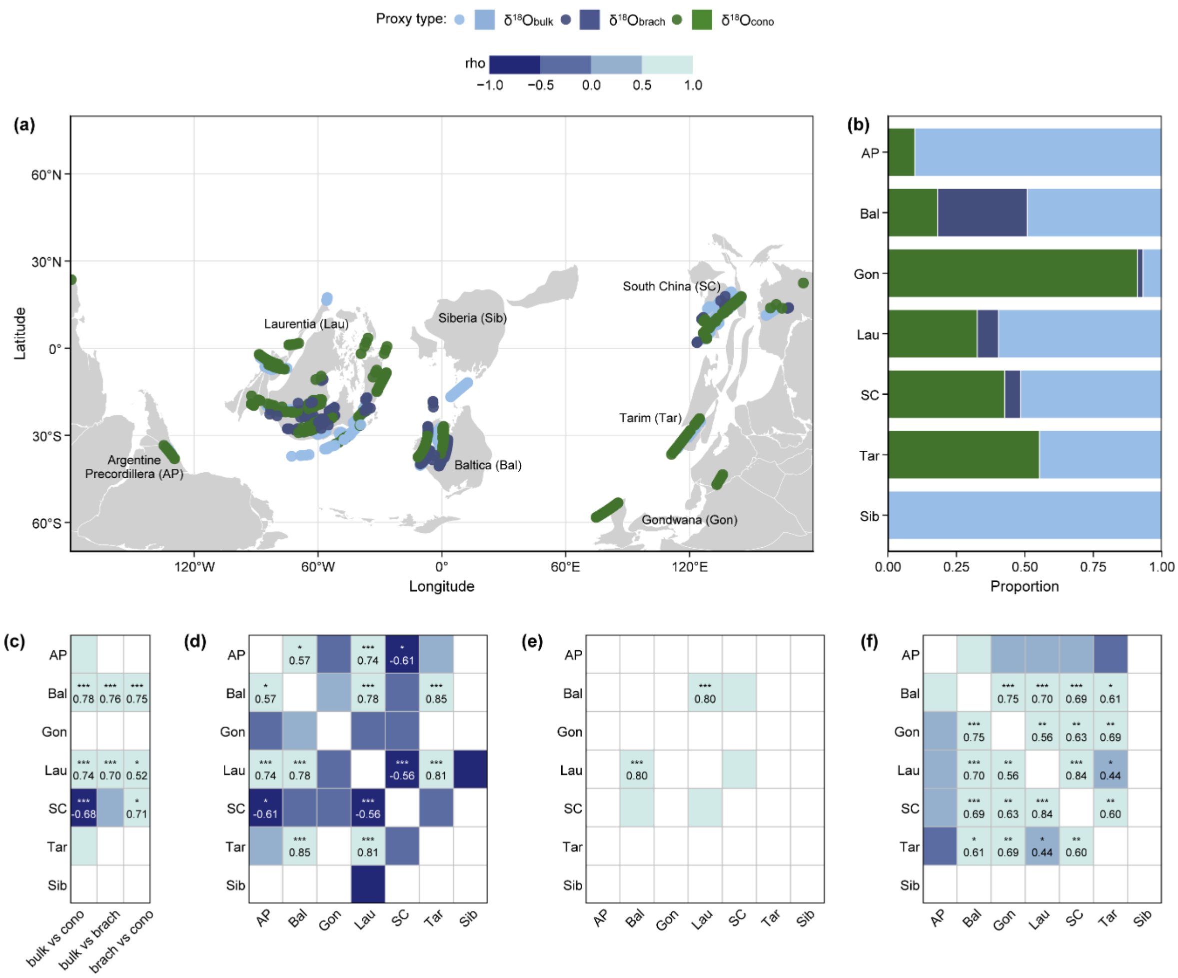

Figure 3. Cross-proxy and cross-paleocontinent consistency of Ordovician δ^{18}O series. (a) Reconstructed sampling positions of bulk-carbonate, brachiopod, and conodont δ^{18}O measurements on the Ordovician paleogeographic map. Colours indicate proxy type. **(b)** Proportional contribution of the three δ^{18}O proxy types within each paleocontinent. AP, Argentine Precordillera; Bal, Baltica; Gon, Gondwana; Lau, Laurentia; SC, South China; Tar, Tarim; Sib, Siberia. **(c)** Spearman correlations among bulk-carbonate, brachiopod, and conodont δ^{18}O series within each paleocontinent. **(d–f)** Spearman correlations among paleocontinents within bulk-carbonate, brachiopod, and conodont δ^{18}O series, respectively. Numbers show correlation coefficients for significant comparisons. Asterisks indicate significance levels: *, **, and *** denote $p < 0.05$, $p < 0.01$, and $p < 0.001$, respectively. Blank cells indicate insufficient temporal overlap or non-significant correlations.

3 Overview of database contents

OrdoTemp database comprises 15,367 entries; each entry represents one individual isotope proxy value associated with metadata (i.e., row), and contains 49 fields (i.e., columns). These fields are grouped into seven categories (Table 2): (1) site and locations, (2) sample and stratigraphic information, (3) age information, (4) proxy and analytical methods, (5) screening information, (6) geochemical information and (7) references.

3.1 Site and location fields

Site and location fields describe where each entry was collected and where that site was positioned in Ordovician palaeogeography. The siteName field records the name of the section, drill core, or outcrop. The location and country fields provide modern geographic context. Modern coordinates are stored as longitude and latitude in decimal degrees using WGS84. The paleolongitude and paleolatitude fields give reconstructed positions based on the PALEOMAP plate model of Scotese and Wright (2018). The paleocontinent field assigns each entry to a broad paleogeographic region using the reconstructed position and published geological context from original literature.

Table 2. Field names and descriptions.

Field name	**Description**
Site and location fields	
siteName	Name of the drill core, section, or outcrop
location	Modern locality of the collection site (e.g., region, province/state, nearby town)
country	Country of the collection site
longitude	Modern longitude of the collection site; negative values indicate the Western Hemisphere (decimal degrees)
latitude	Modern latitude of the collection site; negative values indicate the Southern Hemisphere (decimal degrees)
paleolongitude	Reconstructed paleolongitude of the collection site; negative values indicate the Western Hemisphere (decimal degrees)
paleolatitude	Reconstructed paleolatitude of the collection site; negative values indicate the Southern Hemisphere (decimal degrees)
paleocontinent	Paleocontinent of the reconstructed collection site
Sample and stratigraphic fields	
sampleName	Sample name as reported in the original publication

sampleDepth	Stratigraphic height or depth relative to the source datum (m, unless otherwise reported)
groupFormation	Lithostratigraphic group or formation name
stratigraphicRange	Chronostratigraphic range of the section, core, or outcrop
descriptionOfDepositionalEnvironment	Depositional environment of the measured material
Proxy and analytical fields	
proxyValue	Original isotopic proxy value
correctedProxyValue	Corrected isotopic proxy value used for harmonized analyses, where applicable
unit	Unit or scale of the proxy value (permil_vsmow, permil_vpdb, or permil)
proxyType	Database proxy category (d18O_bulk, d18O_brach, d18O_cono, D47, d18O_bulk_D47paired, d18O_brach_D47paired)
numberOfReplicates	Number of analytical replicates
measuredMaterial	Material subjected to isotopic analysis (e.g., bulk carbonate, brachiopod, conodont)
descriptionOfMeasuredMaterial	Additional description of the measured material (e.g., lithology or fossil taxon)
analyticalTechnique	Method used for isotopic analysis (IRMS or SIMS)
Age fields	
age	Numerical age assigned to the measurement (Ma)
ageConfidenceRatio	Age-confidence interval divided by the duration of the enclosing stage
ageConstraintQuality	Quality category of the age constraint (excellent, good, moderate, poor, unknown, or not available)
biozones	Biozone name(s) used for the age constraint
taxonomicTypeOfBiozone	Taxonomic group defining the biozone (e.g., conodont, chitinozoan, graptolite, trilobite)
ageConstraintReferenceInformation	Evidence used to constrain age (e.g., biostratigraphy, chronostratigraphy, chemostratigraphy, radioisotopic age)
Screening fields	
screeningStatus	Screening status of the measurement (retained, pending, or removed)
removedByScreeningStep	Screening step responsible for removal or pending status
removalReasonDetail	Reason for removal or pending status

Geochemical fields	
Isotopes	Isotope measurements ($\delta^{13}C$, $\delta^{34}S$, $^{87}Sr/^{86}Sr$)
Elemental suites	Elemental concentrations and ratios (Mg/Ca, Mn/Sr, Sr/Ca, Mn, Sr, Fe, Mg, Rb, Si; concentrations in ppm)
Reference fields	
reference	Author-year citation of the original publication
author	Author list of the original publication
year	Year of the original publication
title	Title of the original publication
journal	Journal or source type of the original publication
doi	DOI of the original publication

3.2 Sample and stratigraphic fields

Sample and stratigraphic fields describe the sampling and stratigraphic context of each measurement within a section or core. The sampleName field preserves the label used in the source publication and may not be unique across the database. The sampleDepth field records the reported sampling height or depth, usually in metres unless otherwise stated. The groupFormation and stratigraphicRange fields link each measurement to lithostratigraphic and chronostratigraphic information. The descriptionOfDepositionalEnvironment field records the reported depositional setting extracted from original literature where available.

3.3 Age fields

Age fields provide the temporal framework for each measurement. The age field gives the assigned numerical age in Ma. The biozones, taxonomicTypeOfBiozone, and ageConstraintReferenceInformation fields record the stratigraphic information used to assign that age, such as conodont, chitinozoan, graptolite, or trilobite biozones, chronostratigraphy, chemostratigraphy, primary-source age information, or radioisotopic dates. The ageConfidenceRatio and ageConstraintQuality fields describe the uncertainty of the age assignment.

3.4 Proxy and analytical fields

Proxy and analytical fields store the measured isotope values and the measurement information. The proxyValue field preserves the value reported in the source publication. The correctedProxyValue field stores the harmonised value used for analysis where a correction was applied, such as conodont $\delta^{18}O$ standardisation. The unit field records the scale of the value, including VPDB, VSMOW, or per mil clumped-isotope units.

The proxyType field distinguishes the internal proxy labels used in the database, including bulk-carbonate $\delta^{18}O$, brachiopod $\delta^{18}O$, conodont $\delta^{18}O$, Δ_{47}, and paired $\delta^{18}O$ values associated with Δ_{47} analyses. The measuredMaterial and descriptionOfMeasuredMaterial fields describe the measured phase or fossil material. The numberOfReplicates and conodontMeasurementTechnique fields provide additional analytical context where available.

Supporting geochemical information is also summarised in Table 2 under geochemical fields. Isotopes include $\delta^{13}C$, $\delta^{34}S$, and $^{87}Sr/^{86}Sr$, whereas elemental suites include Mg/Ca, Mn/Sr, Sr/Ca, Mn, Sr, Fe, Mg, Rb, and Si.

3.5 Screening fields

Screening fields record the result of the quality-control workflow for each measurement. The screeningStatus field classifies each measurement as retained, pending, or removed. Retained measurements passed the implemented workflows. Pending measurements lack enough support for final acceptance. Removed measurements failed one or more screening criteria but remain in the database for transparency and possible alternative use.

The removedByScreeningStep field identifies the main step responsible for removal or pending status, such as age, lithology, depositional environment, petrography and geochemistry, quantitative screening, or consistency screening. The removalReasonDetail field gives a row-level explanation.

3.6 Data source field

The reference field includes author, year, title, journal, and DOI. These fields allow users to cite the original publications when producing derived datasets or interpretations. Reference and metadata fields were standardised with scripts to harmonise whitespace, categorical terms, DOI formats, and source labels while preserving complete bibliographic information. Each entry in the main sheet is linked to the reference sheet through the ‘reference’ field, and the ‘doi’ field provides a direct route for source verification through Crossref.

4 Technical validations

OrdoTemp database was checked through manual review and automated validation to improve internal consistency, traceability, and reuse. The validation focused on source links, geographic and paleogeographic information, age control, duplicate entries, proxy-specific fields, analytical information, and screening-status documentation.

4.1 Reference and source verification

Reference labels were checked between the two sheets to confirm that each source label in the main sheet corresponds to a source-publication record. DOI and source-link fields were also reviewed. Where a source link is not a formal DOI, it was retained as a plain URL. These checks support data provenance and allow users to trace entries back to their original publications or source documents.

4.2 Geographic coordinate verification

Modern longitude and latitude values were checked to confirm that they fall within valid coordinate ranges. Coordinates were compared with reported locality and country information, and sampling locations were inspected against modern geographic context. The country field records the sovereign state of the modern locality. For example, entries from Greenland are listed under Denmark.

4.3 Paleocoordinate validation

Reconstructed paleolongitude and paleolatitude values were checked for numerical range and consistency with assigned age and paleocontinent. Paleocontinent names were standardised to avoid inconsistent spellings or formatting. Some entries with numerical ages do not have reconstructed paleocoordinates because the reconstruction returned invalid placeholder values. These entries were left blank in the paleocoordinate fields.

4.4 Duplicate and metadata checks

Duplicate entries were checked by comparing database rows. Exact duplicates were removed after source-level review. Proxy values and auxiliary geochemical fields were inspected to identify malformed values, formula residues, and extreme values. Missing metadata were also reviewed. Some entries lack siteName, sampleName, descriptionOfMeasuredMaterial, or auxiliary geochemical information because these details were not reported in the original publications. These fields were retained as blank or NaN. Negative values in sampleDepth were also retained where they represent stratigraphic height relative to the datum used in the source publication.

4.5 Age-constraint validation

Age fields were checked against the stratigraphic information recorded in the database and the Geological Time Scale 2020. Numerical ages, biozone assignments, age-reference information, and age-quality classes were reviewed for internal consistency. The chronostratigraphic and biostratigraphic framework was also independently reviewed by biostratigraphy specialists (Yiying Deng and Linna Zhang), and numerical ages were corrected where needed.

The ageConfidenceRatio field was checked separately. For some fossil and clumped-isotope entries, a precise ratio cannot be calculated from the available source information, although the assigned numerical age falls within the reported stage. These entries are recorded as <1 and assigned ageConstraintQuality = moderate. This notation should be treated as a qualitative age-confidence flag. Entries with limited age evidence were assigned to the pending class when available information is insufficient for either removal or retention.

4.6 Proxy-specific, analytical and screening-status validation

Proxy fields were checked for consistency among proxyType, unit, proxyValue, correctedProxyValue, and analyticalTechnique. Conodont $\delta^{18}O$ values received additional validation because they required standardisation. SIMS conodont values were checked against the reported values and the applied correction. Non-conodont proxy values were checked to confirm that correctedProxyValue was not changed unless a harmonisation step was intended. The purpose of this validation is therefore to check whether the screening outcome is documented consistently and transparently.

5 General database statistics

The 15,367 data entries in the *OrdoTemp* database, of which 5,223 (34.0%) were retained, 650 (4.2%) remain pending, and 9,494 (61.8%) were removed (Table 3). Bulk-carbonate $\delta^{18}O$ constitutes the largest proxy category, comprising 12,171 values (79% of the database). Of these, 2,769 (22.8%) were retained, 525 (4.3%) remain pending, and 8,877 (72.9%) were removed. Of the 1,194 brachiopod $\delta^{18}O$ values, 624 (52.3%) were retained, and 570 (47.7%) were removed. Almost all conodont $\delta^{18}O$ values show the highest retention fraction: 1,750 of 1,781 values (98.3%) were retained, and only 31 (1.7%) were removed. Of the 221 Δ_{47} data, 80 (36.2%) were retained, 125 (56.6%) remained pending, and 16 (7.2%) were removed (Table 3).

Among all removal screening steps for isotopic proxy data, petrographic and geochemical screening accounted for the largest proportion of removals (3,622 data; 38%), followed by quantitative screening criteria (2,057; 22%), age constraints (1,936; 20%) and lithological screening (1,464; 15%). Depositional-environment and consistency screening removed a further 265 (3%) and 150 (2%) data, respectively. All 525 pending bulk-carbonate $\delta^{18}O$ data resulted from consistency screening, whereas the remaining 125 pending data are Δ_{47} measurements awaiting further age uncertainty evaluation (Tables 3–4).

The ages of all retained proxy data were constrained predominantly by biostratigraphy (2,691 values; 52%) and chronostratigraphy (1,960; 38%). Smaller subsets were constrained using chemostratigraphy (239; 5%), combined biostratigraphy and chemostratigraphy (199; 4%), age information reported in the primary references (116; 2%), or combined biostratigraphy and chronostratigraphy (18; <1%; Table 5). Most retained data entries have moderate (3,015; 58%) or excellent (2,046; 39%) age quality, whereas only 46 (1%) were classified as good and 116 (2%) as unknown (Table 6).

Table 3. Number of proxy data by type and screening status in the *OrdoTemp* database.

Proxy type	All entries		Retained entries		Pending entries		Removed entries	
	N	Proportion	N	Proportion	N	Proportion	N	Proportion
$\delta^{18}O_{bulk}$	12,171	79%	2,769	53%	525	81%	8,877	94%
$\delta^{18}O_{brach}$	1,194	8%	624	12%	0	0%	570	6%
$\delta^{18}O_{cono}$	1,781	12%	1,750	34%	0	0%	31	0%
Δ_{47}	221	1%	80	2%	125	19%	16	0%
Total	15,367		5,223		650		9,494	

Table 4. Number of removed and pending data by screening step in the *OrdoTemp* database.

Screening step	Removed entries		Pending entries	
	N	Proportion	N	Proportion
age	1,936	20%	125	19%
lithology	1,464	15%	0	0%
depositional_environment	265	3%	0	0%
petrography_geochem	3,622	38%	0	0%
quantitative	2,057	22%	0	0%
consistency	150	2%	525	81%
Total	9,494		650	

Table 5. Number of retained data by age-constraint reference information in the *OrdoTemp* database.

Age-constraint reference information	Retained entries	
	N	Proportion
biostratigraphy	2,691	52%
chronostratigraphy	1,960	38%
biostratigraphy and chemostratigraphy	199	4%
biostratigraphy and chronostratigraphy	18	0%
chemostratigraphy	239	5%
age information from primary references	116	2%
Total	5,223	

Table 6. Number of retained data by age-constraint quality in the *OrdoTemp* database.

Age-constraint quality	Retained entries	
	N	Proportion
excellent	2,046	39%
good	46	1%
moderate	3,015	58%
unknown	116	2%
Total	5,223	

5.1 Geochemical characteristics across data-screening outcomes

5.1.1 $\delta^{18}O$ data

Figure 4 shows the temporal distribution of $\delta^{18}O$ values across the Ordovician by proxy type and screening status. Here, our retained bulk-carbonate $\delta^{18}O$ values show relatively coherent temporal patterns as those from fossils, indicating that the screening reduced the influence of isolated anomalous values and improved the stratigraphic consistency of the dataset. Whereas removed bulk-carbonate $\delta^{18}O$ values are more scattered and include both unusually low and high values, consistent with their heterogeneous diagenetic preservation states and screening failures (Fig. 4a).

There are some concerns: given that oxygen dominates in natural fluids, the temperature during diagenetic stabilization could not be identical to the temperature during the precipitation of the precursor. It is likely that the well-preserved bulk-carbonate $\delta^{18}O$ values are not completely the same as prior to burial (Banner and Hanson, 1990; Marshall, 1992; Jacobsen and Kaufman, 1999). In this study, however, we observed that the retained $\delta^{18}O$ values derived from well-preserved low-Mg calcite fossil material greatly overlap with the retained $\delta^{18}O_{bulk}$ values (Fig. 4a), which suggests the factor has little effect on our well-screened $\delta^{18}O_{bulk}$ dataset.

In addition, in our database, a small subset of retained carbonate $\delta^{18}O$ values is paired with published Δ_{47} measurements from well-preserved micrites or brachiopods (Finnegan et al., 2011; Bergmann et al., 2018; Goldberg et al., 2021; Barney and Grossman, 2022; Thiagarajan et al., 2024). These samples are generally interpreted as preserving primary or only slightly modified $\delta^{18}O$ signals because Δ_{47}-temperature, pair-measured mineral $\delta^{18}O$ and calculated fluid $\delta^{18}O$ data suggest that post-depositional diagenesis could occur in rock-buffer close systems with low water-to-rock ratios where primary $\delta^{18}O$ compositions were minimally altered (Brand and Veizer, 1980; Banner and Hanson, 1990; Marshall, 1992; Jacobsen and Kaufman, 1999; Bergmann et al., 2018; Goldberg et al., 2021; Thiagarajan et al., 2024). Consistently, here, these retained carbonate $\delta^{18}O$ data (including from bulk carbonates and brachiopod shells) and phosphate $\delta^{18}O$ data from conodont fossils show broadly similar temporal patterns to this clumped-paired carbonate $\delta^{18}O$ ($\delta^{18}O_{clump}$) subset (Fig. 4a). This agreement suggests that post-depositional modification was limited, likely because screening preferentially retained carbonates affected only by rock-buffered diagenesis at low water-to-rock ratios, under which the rock oxygen reservoir dominated the isotopic mass balance (Brand and Veizer, 1980; Banner and Hanson, 1990; Marshall, 1992; Jacobsen and Kaufman, 1999). This observation also provides independent support that the retained dataset captures a common first-order Ordovician $\delta^{18}O$ pattern rather than an archive-specific diagenetic signal.

The proportions of retained, pending, and removed $\delta^{18}O$ measurements show considerable variability among 1 Myr time bins across the Ordovician (Fig. 4b). Removed measurements account for a large fraction of the compiled dataset in many intervals, whereas retained records are primarily composed of bulk-carbonate $\delta^{18}O$ data. Conodont, brachiopod, and carbonate clumped isotope (Δ_{47}) measurements represent smaller but temporally variable contributions to the retained dataset.

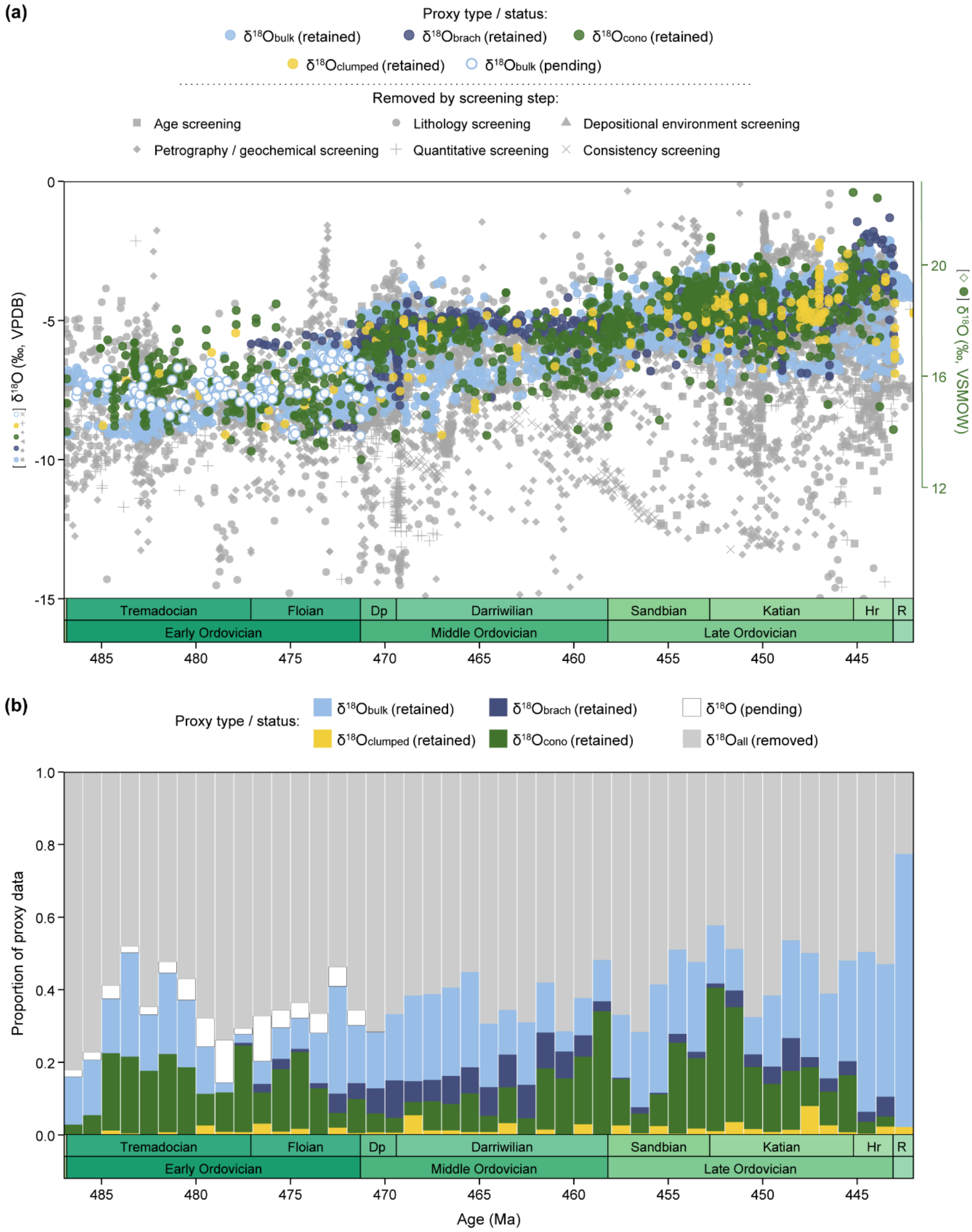

Figure 4. Temporal distribution of the $\delta^{18}O$ dataset through the Ordovician. (a) Retained measurements are colored by proxy type; pending measurements are open symbols, and all removed measurements are grey, with symbol shapes showing the screening steps. The $\delta^{18}O_{clumped}$ values come from carbonate samples also paired with Δ_{47} measurements. Carbonate $\delta^{18}O$ values use the left VPDB axis, and phosphate $\delta^{18}O$ values use the independent

right VSMOW axis. **(b)** Proportions of retained, pending and removed measurements in 1-myr time bins. Dp, Dapingian; Hr, Hirnantian.

5.1.2 Geochemical metadata

We compared characteristics of retained, pending and removed geochemical metadata to assess whether the quality-control procedures preferentially excluded records exhibiting potential signals of diagenetic alteration (Fig. 5). In *OrdoTemp*, retained bulk-carbonate records generally had low Mn/Sr, Mn, Fe and Mg/Ca values (Fig. 5a,5c, 5e and 5g). Pending records largely overlapped the retained population but covered a broader range, indicating that their preservation could not be resolved from the available geochemical evidence alone. By contrast, the removed data entries showed broader, right-skewed distributions, with Mn/Sr exceeding 10, Fe approaching 60,000 and Mg/Ca approaching 200 (Fig. 5a, 5e and 5g), consistent with diagenetic alteration (Brand and Veizer, 1980; Veizer et al., 1992a; Veizer et al., 1992b; Denison et al., 1994; Banner, 1995; Brand et al., 2012; Garbelli et al., 2012). Available $^{87}Sr/^{86}Sr$ measurements occurred only among removed bulk-carbonate data entries and were concentrated mainly between 0.710 and 0.713 (Fig. 5f). These radiogenic ratios are substantially higher than published Ordovician seawater values and are consistent with post-depositional modification or contamination by radiogenic, non-carbonate components (Gorokhov et al., 1995; Ovchinnikova et al., 1995; Fairchild et al., 2018; Shields and Veizer, 2002; Shields et al., 2003; Chen et al., 2022b). Importantly, retained bulk carbonates and retained brachiopod records generally overlapped within the low-value portions of the Mn/Sr, Mn, Fe and Mg/Ca distributions (Fig. 5a, 5c, 5e and 5g).

Compared to brachiopod Mn/Sr, Mn, Sr, Fe and Mg/Ca, brachiopod Sr/Ca provided the clearest contrast: retained entries were concentrated at approximately 1.6–2.1, whereas removed records spanned approximately 0.2–2.3 and included numerous values below 1.5 (Fig. 5b). This low-Sr/Ca tail is consistent with Sr loss during recrystallisation and therefore supports the exclusion of poorly preserved shells in our database. The smaller Δ_{47} dataset was generally associated with low Mn/Sr, Mn and Fe values, although its limited sample size precludes a robust comparison among screening outcomes (Fig. 5a, 5c and 5e). The $\delta^{13}C$–$\delta^{18}O$ crossplot provided additional support for these classifications and showed a similar pattern: retained bulk-carbonate and brachiopod records formed relatively compact, overlapping clusters, whereas removed bulk-carbonate records occupied a broader field, particularly towards lower $\delta^{18}O$ values (Fig. 5h). Pending data entries overlapped the retained clusters but extended into the field occupied by removed records. Overall, these results above suggest that these screening steps used here effectively retained records displaying geochemical characteristics consistent with better preservation, while preferentially excluding records exhibiting multiple potential indicators of diagenetic alteration.

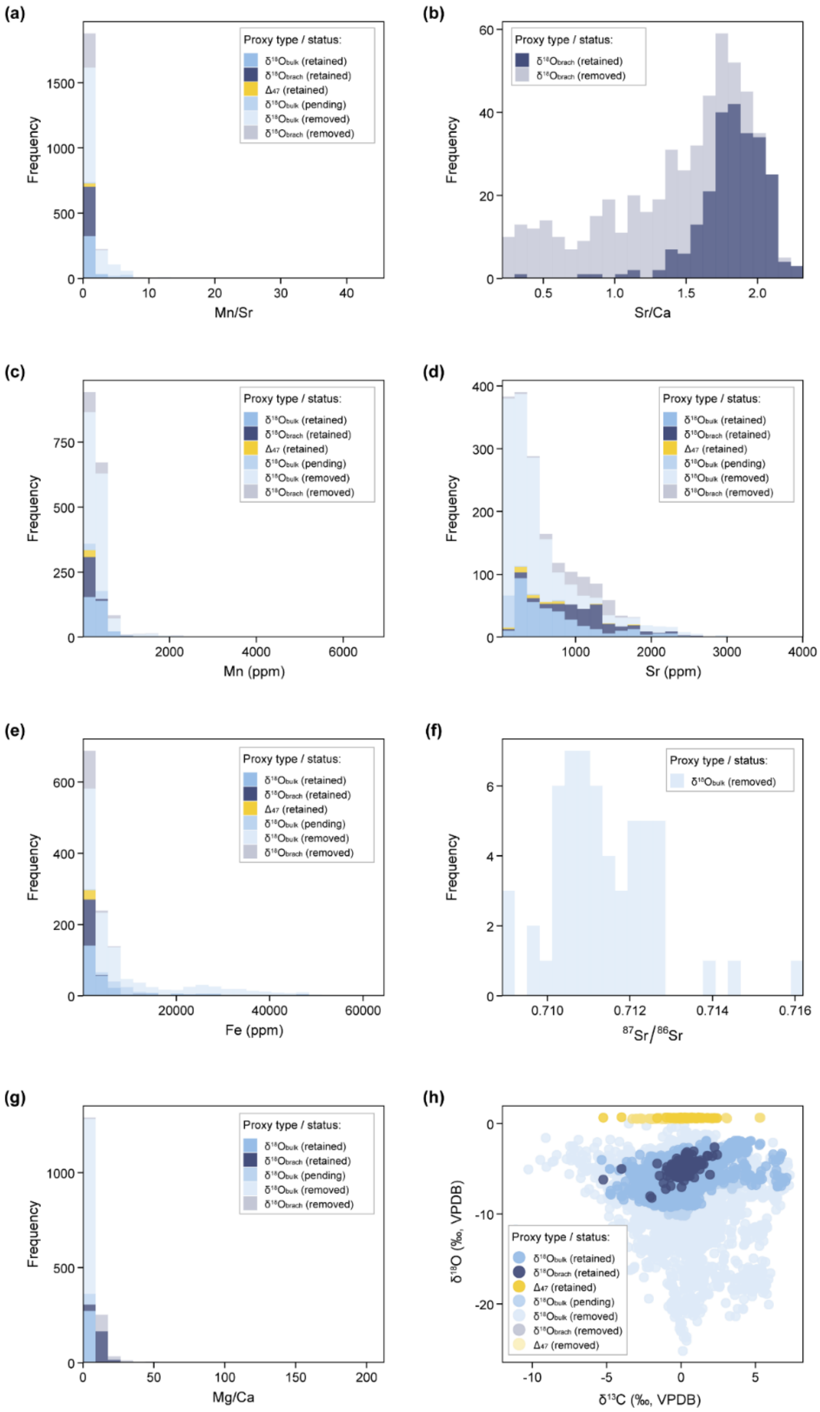

Figure 5. Geochemical distributions across proxy type and screening status. (a–g) Frequency distributions of Mn/Sr, Sr/Ca, Mn, Sr, Fe, $^{87}Sr/^{86}Sr$ and Mg/Ca, respectively. **(h)** Crossplot of $\delta^{13}C$–$\delta^{18}O$ values. Colours distinguish $\delta^{18}O_{bulk}$, $\delta^{18}O_{brach}$ and Δ_{47} data classified as retained, pending or removed status.

5.2 Temporal resolution of isotopic values

The temporal-resolution analysis includes 4,250 retained Ordovician oxygen-isotope data (excluding Δ_{47}-only data). The temporal resolution of these well-screened Ordovician proxy data was calculated by subtracting the older age from the younger of two adjacent unique ages. The temporal resolution ranges from 4.7 kyr to 1293.7 kyr (5th and 95th), with a median value of 61.8 kyr (Fig. 6). However, this calculation exaggerates the precision of the age constraint used in this study. We therefore recommend using time bins from 1 Myr (roughly the best resolution of Ordovician biozonation; Goldman et al., 2020) to 0.1 Myr for paleotemperature reconstruction.

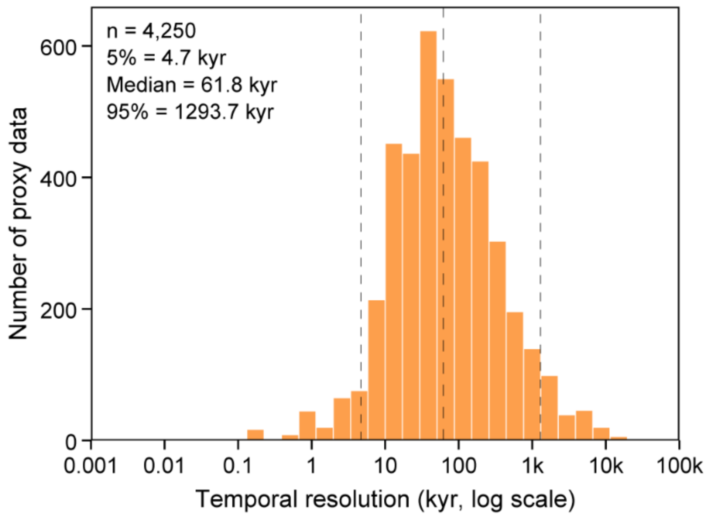

Figure 6. Temporal resolution of retained $\delta^{18}O$ data in the *OrdoTemp* database. Temporal resolution is reported in kyr. Temporal resolution was calculated as the minimum interval between adjacent unique-age observations within each individual record. The histogram presents the distribution of temporal resolutions on a logarithmic kyr scale. Dashed vertical lines indicate the 5th percentile, median, and 95th percentile values.

5.3 Spatio-temporal trends in isotopic proxy values

The 5,223 retained Ordovician proxy entries are strongly concentrated in Laurentia (3,449; 66%) and Baltica (1,075; 21%). The remaining entries are distributed across South China (231; 4%), Tarim (179; 3%), the Argentine Precordillera (153; 3%), and Gondwana (136; 3%) (Table. 7).

Table 7. Number of retained data by paleocontinents in the *OrdoTemp* database.

Paleocontinents	Retained entries	
	N	Proportion

Laurentia	3,449	66%
Baltica	1,075	21%
South China	231	4%
Tarim	179	3%
Argentine Precordillera	153	3%
Gondwana	136	3%
Total	5,223	

Across the 487–443 Ma interval, retained carbonate $\delta^{18}O$ data (n = 3,254) are concentrated between the palaeoequator and 40° S, whereas phosphate $\delta^{18}O$ data (n = 1,750) span a broader range from approximately 30° N to 60° S and both archives generally shift towards higher $\delta^{18}O$ values through time. (Fig. 7a and 7b). At comparable ages, lower $\delta^{18}O$ values generally occur at low palaeolatitudes, whereas higher values are more common at southern mid- to high palaeolatitudes, consistent with the patterns of latitudinal temperature gradients (Fig. 7a and 7b).

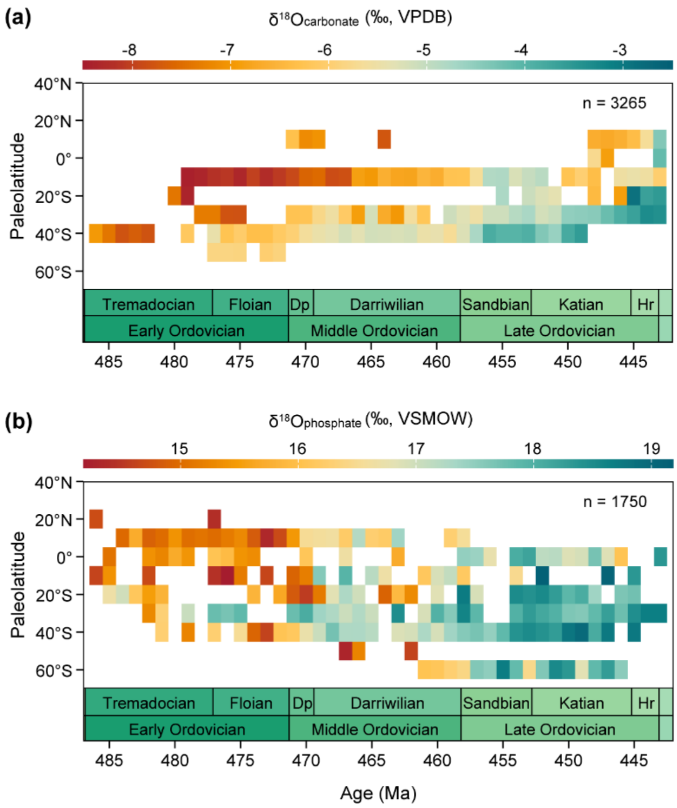

Figure 7. Temporal and latitudinal distribution of Ordovician oxygen isotope proxy data. (a) Spatial distribution of retained carbonate $\delta^{18}O$ values (including bulk carbonate, brachiopod carbonate). **(b)** Spatial distribution of retained conodont

phosphate $\delta^{18}O$ values. Data are aggregated into 1 Myr × 10° paleolatitude bins, and colours represent the mean $\delta^{18}O$ values within each bin. The number of retained observations (n) is shown in each panel. Dp, Dapingian; Hr, Hirnantian.

6 Usage notes

6.1 Informed user notice

Users of *OrdoTemp* should be aware that isotope proxy values and paleotemperature estimates contain several sources of uncertainty. These include analytical uncertainty, archive-specific vital effects, interspecific or intraspecific differences in fossil-shell oxygen isotope values, uncertainties introduced by temperature equations, uncertainty in seawater $\delta^{18}O$, ice-volume effects on seawater $\delta^{18}O$, and spatial heterogeneity in seawater $\delta^{18}O$.

6.2 Applying the database to Ordovician temperature studies

This dataset provides a comprehensive framework for investigating Ordovician climate system changes in the context of the GOBE and LOME. It enables studies of: (1) global-scale temporal and spatial patterns of Ordovician climate variability; (2) regional expressions of climate change across different palaeogeographic settings; (3) evaluation and validation of climate model simulations; and (4) potential relationships among climate dynamics, the GOBE, and the LOME. Beyond temperature reconstruction, *OrdoTemp* can guide multi-proxy studies of Ordovician environmental change. Retained carbonate and fossil $\delta^{18}O$ records are useful targets for paired measurements such as $\delta^{13}C$, $\delta^{34}S$, trace elements, and clumped isotopes, to examine links among climate, seawater chemistry, carbonate preservation, diagenesis, sea-level change, and Ordovician biological events. Where the $\delta^{18}O$ records can be paired with an independent temperature archive, they may be used to constrain seawater $\delta^{18}O$. These constraints may also aid interpretation of coeval siliciclastic records by helping distinguish primary environmental signals from later diagenetic alteration.

6.3 A reproducible screening workflow for deep-time bulk-carbonate $\delta^{18}O$ data

A major purpose of *OrdoTemp* is to provide a transparent workflow for using deep-time bulk-carbonate $\delta^{18}O$ data. Deep-time (e.g., the Palaeozoic) bulk-carbonate records are abundant but more susceptible to diagenetic alteration. This workflow provides a reproducible framework for deep-time $\delta^{18}O$ proxy synthesis in the future.

7 Data availability

The *OrdoTemp* database is freely available and can be found at Dryad https://doi.org/10.5061/dryad.2jm63xt6h (Ma et al., 2026).

Author contributions. XLM, JXF and IPM conceptualised the study. XLM, YYD, LNZ, TI, JXF and IPM contributed to data curation. XLM, JXF, and IPM conducted investigations and developed the methodology. XLM performed the writing – original draft preparation. All authors contributed to writing – review and editing. JXF and IPM provided supervision and project administration.

Competing interests. The authors declare no competing interests.

Acknowledgements. We thank Suyun Zhang and Yexuan Zhang for their help in collecting data. We also thank Xiaofang Teng for helping to constrain the age of the isotopic proxy data from the fossil shells, and Shengchao Yang, Yukun Shi and Norman MacLeod for their valuable suggestions during the study.

Financial support. This work was supported by the National Natural Science Foundation of China (grant. no. 92255301) and the International Science and Technology Cooperation Program of Jiangsu (grant no. BZ2023068). This paper is a contribution to the "Deep-time Digital Earth" Big Science Program, the IGCP 735 Project "Rocks and the Rise of Ordovician Life" and the OneStratigraphy Database.

References

Ainsaar, L., Meidla, T., and Martma, T.: Evidence for a widespread carbon isotopic event associated with late Middle Ordovician sedimentological and faunal changes in Estonia, Geological Magazine, 136, 49-62, 10.1017/s001675689900223x, 1999.

Al-Aasm, I. S. and Veizer, J.: Chemical stabilization of low-Mg calcite: an example of brachiopods, Journal of Sedimentary Research, 52, 1101-1109, 10.1306/212F80E4-2B24-11D7-8648000102C1865D, 1982.

Albanesi, G. L., Barnes, C. R., Trotter, J. A., Williams, I. S., and Bergström, S. M.: Comparative Lower-Middle Ordovician conodont oxygen isotope palaeothermometry of the Argentine Precordillera and Laurentian margins, Palaeogeography, Palaeoclimatology, Palaeoecology, 549, 109115, https://doi.org/10.1016/j.palaeo.2019.03.016, 2020.

Allan, J. R. and Matthews, R. K.: Isotope signatures associated with early meteoric diagenesis, Sedimentology, 29, 797-817, https://doi.org/10.1111/j.1365-3091.1982.tb00085.x, 1982.

Alroy, J.: The shifting balance of diversity among major marine animal groups, Science, 329, 1191–1194, https://doi.org/10.1126/science.1189910, 2010.

Avila, T. D., Saltzman, M. R., Adiatma, Y. D., Joachimski, M. M., Griffith, E. M., and Olesik, J. W.: Role of seafloor production versus continental basalt weathering in Middle to Late Ordovician seawater $^{87}Sr/^{86}Sr$ and climate, Earth and Planetary Science Letters, 593, 117641, https://doi.org/10.1016/j.epsl.2022.117641, 2022.

Azmy, K. and Jin, J.: Geochemistry of Late Ordovician dalmanelloid brachiopods from Laurentia: testing the effects of paleolatitudinal gradient, Canadian Journal of Earth Sciences, 56, 235-244, 10.1139/cjes-2018-0181, 2019.

Azmy, K., Veizer, J. N., Bassett, M. G., and Cooper, P.: Oxygen and carbon isotopic composition of Silurian brachiopods: Implications for coeval seawater and glaciations, GSA Bulletin, 110, 1499-1512, 10.1130/0016-7606(1998)110<1499:OACICO>2.3.CO2, 1998.

Azmy, K., Stouge, S., Brand, U., Bagnoli, G., and Ripperdan, R.: High-resolution chemostratigraphy of the Cambrian-Ordovician GSSP: Enhanced global correlation tool, Palaeogeography Palaeoclimatology Palaeoecology, 409, 135-144, 10.1016/j.palaeo.2014.05.010, 2014.

Banner, J. L.: Application of the trace element and isotope geochemistry of strontium to studies of carbonate diagenesis, Sedimentology, 42, 805-824, https://doi.org/10.1111/j.1365-3091.1995.tb00410.x, 1995.

Banner, J. L. and Hanson, G. N.: Calculation of simultaneous isotopic and trace element variations during water-rock interaction with applications to carbonate diagenesis, Geochimica et Cosmochimica Acta, 54, 3123-3137, https://doi.org/10.1016/0016-7037(90)90128-8, 1990.

Banner, J. L. and Kaufman, J.: The isotopic record of ocean chemistry and diagenesis preserved in non-luminescent brachiopods from Mississippian carbonate rocks, Illinois and Missouri, GSA Bulletin, 106, 1074-1082, 10.1130/0016-7606(1994)106<1074:TIROOC>2.3.CO;2, 1994.

Barney, B. B. and Grossman, E. L.: Reassessment of ocean paleotemperatures during the Late Ordovician, Geology, 50, 572-576, 10.1130/G49422.1, 2022.

Bartlett, R., Elrick, M., Wheeley, J. R., Polyak, V., Desrochers, A., and Asmerom, Y.: Abrupt global-ocean anoxia during the Late Ordovician–early Silurian detected using uranium isotopes of marine carbonates, Proceedings of the National Academy of Sciences, 115, 5896-5901, 10.1073/pnas.1802438115, 2018.

Bassett, D., Macleod, K. G., Miller, J. F., and Ethington, R. L.: Oxygen isotopic composition of biogenic phosphate and the temperature of Early Ordovician seawater, PALAIOS, 22, 98-103, 10.2110/palo. 2005.p05-089r, 2007.

Bates, N. R. and Brand, U.: Secular variation of calcium carbonate mineralogy; an evaluation of ooid and micrite chemistries, Geologische Rundschau, 79, 27-46, 10.1007/BF01830446, 1990.

Bergmann, K., Boekelheide, N., Clarke, J., Cantine, M., Wilcots, J., Anderson, N., Jost, A., Laub, O., Drozd, J., Goldberg, S., Mackey, T., Meyer, F., and Eyster, A.: Temperature: a key driver of Earth's habitability over the last billion years, 10.1002/essoar.10511918.3, 2022.

Bergmann, K. D., Finnegan, S., Creel, R., Eiler, J. M., Hughes, N. C., Popov, L. E., and Fischer, W. W.: A paired apatite and calcite clumped isotope thermometry approach to estimating Cambro-Ordovician seawater temperatures and isotopic composition, Geochimica et Cosmochimica Acta, 224, 18-41, https://doi.org/10.1016/j.gca.2017.11.015, 2018.

Bergmann, K. D., Macdonald, F. A., and Swanson-Hysell, N. L.: The Causes and Consequences of Ordovician Cooling, Annual Review of Earth and Planetary Sciences, 53, 651-685, https://doi.org/10.1146/annurev-earth-040523-114630, 2025.

Boggs, J. S.: Diagenesis of carbonate rocks, in: Petrology of Sedimentary Rocks, 2 ed., edited by: Boggs, J. S., Cambridge University Press, Cambridge, 408-458, DOI: 10.1017/CBO9780511626487.012, 2009.

Bond, D. P., and Grasby, S. E.: Late Ordovician mass extinction caused by volcanism, warming, and anoxia, not cooling and glaciation, Geology, 48 (8), 777–781, https://doi.org/10.1130/G47377.1, 2020.

Brand, U.: Carbon, oxygen and strontium isotopes in Paleozoic carbonate components: an evaluation of original seawater-chemistry proxies, Chemical Geology, 204, 23-44, https://doi.org/10.1016/j.chemgeo.2003.10.013, 2004.

Brand, U. and Veizer, J.: Chemical diagenesis of a multicomponent carbonate system; 1, Trace elements, Journal of Sedimentary Research, 50, 1219-1236, 10.1306/212F7BB7-2B24-11D7-8648000102C1865D, 1980.

Brand, U., Jiang, G., Azmy, K., Bishop, J., and Montañez, I. P.: Diagenetic evaluation of a Pennsylvanian carbonate succession (Bird Spring Formation, Arrow Canyon, Nevada, U.S.A.) — 1: Brachiopod and whole rock comparison, Chemical Geology, 308-309, 26-39, https://doi.org/10.1016/j.chemgeo.2012.03.017, 2012.

Brand, U., Logan, A., Bitner, M., Erika, G., Azmy, K., and Buhl, D.: What is the ideal proxy of Paleozoic seawater chemistry?, Memoirs of the Association of Australasian Palaeontologists, 41, 9-24, 2011.

Brookfield, M. E. and Hannigan, R. E.: Carbon and oxygen isotope variations in shell beds from the Upper Ordovician (mid-Cincinnatian: Maysvillian to early Richmondian) of Ontario: Evaluation of the Warm Saline Deep Ocean hypothesis, paleoceanographic changes, and Milankovitch orbital cycles in the transition to the Hirnantian glaciation, Palaeogeography, Palaeoclimatology, Palaeoecology, 577, 110528, https://doi.org/10.1016/j.palaeo.2021.110528, 2021.

Bruland, K. W., Middag, R., and Lohan, M. C.: 8.2 - Controls of Trace Metals in Seawater, in: Treatise on Geochemistry (Second Edition), edited by: Holland, H. D., and Turekian, K. K., Elsevier, Oxford, 19-51, https://doi.org/10.1016/B978-0-08-095975-7.00602-1, 2014.

Buggisch, W., Joachimski, M. M., Lehnert, O., Bergström, S. M., Repetski, J. E., and Webers, G. F.: Did intense volcanism trigger the first Late Ordovician icehouse?, Geology, 38, 327-330, 10.1130/G30577.1, 2010.

Calner, M., Bockelie, J., Rasmussen, C., Calner, H., Lehnert, O., and Joachimski, M.: Carbon isotope chemostratigraphy and sea- level history of the Hirnantian Stage (uppermost Ordovician) in the Oslo-Asker district, Norway, Geological Magazine, 10.1017/S0016756821000546, 2021.

Canfield, D. E. and Thamdrup, B.: Towards a consistent classification scheme for geochemical environments, or, why we wish the term 'suboxic' would go away, Geobiology, 7, 385-392, https://doi.org/10.1111/j.1472-4669.2009.00214.x, 2009.

Chai, F.: Study on Paleozoic sedimentary facies and favorable area evaluation in lower Yangtze basin, Reservoir Evaluation and Development, 9, 7-12, 2019.

Chen, C., Shi, X. Y., Zhang, W. H., and Tian, X. L.: The Guttenberg $\delta^{13}C$ excursion (GICE) and paleoclimate change recorded in the early Late Ordovician carbonate succession of the Ordos Basin, Northern China, Journal of Asian Earth Sciences, 231, 10.1016/j.jseaes.2022.105211, 2022a.

Chen, X., Zhou, Y., and Shields, G. A.: Progress towards an improved Precambrian seawater $^{87}Sr/^{86}Sr$ curve, Earth-Science Reviews, 224, 103869, https://doi.org/10.1016/j.earscirev.2021.103869, 2022b.

Cramer, B. D. and Jarvis, I.: Chapter 11 - Carbon Isotope Stratigraphy, in: Geologic Time Scale 2020, edited by: Gradstein, F. M., Ogg, J. G., Schmitz, M. D., and Ogg, G. M., Elsevier, 309-343, https://doi.org/10.1016/B978-0-12-824360-2.00011-5, 2020.

Denison, R. E., Koepnick, R. B., Fletcher, A., Howell, M. W., and Callaway, W. S.: Criteria for the retention of original seawater 87Sr86Sr in ancient shelf limestones, Chemical Geology, 112, 131-143, https://doi.org/10.1016/0009-2541(94)90110-4, 1994.

Deng, Y. Y., Fan, J. X., Zhang, S. H., Fang, X., Chen, Z. Y., Shi, Y. K., Wang, H. W., Wang, X. B., Yang, J, Hou, X. D., Wang, Y., Zhang, Y. D., Chen, Q., Yang, A. H., Fan, R., Dong, S. C., Xu, H. Q., and Shen, S. Z.: Timing and patterns of the Great Ordovician Biodiversification Event and Late Ordovician mass extinction: Perspectives from South China. Earth-Science Reviews, 103743, https://doi.org/10.1016/j.earscirev.2021.103743, 2021.

Dent, L., Normore, L., Sullivan, N. B., Zhen, Y. Y., and Forbes, A.: First record of lower - Middle Ordovician (Tremadocian - Dapingian) carbon isotope $\delta^{13}C_{carb}$ chemostratigraphy in the Canning Basin, Western Australia; calibrated with geochronology/biostratigraphy and implications for global correlations, Palaeogeography Palaeoclimatology Palaeoecology, 573, 10.1016/j.palaeo.2021.110411, 2021.

Diamond, C. W.: Ocean oxygenation during the Middle Ordovician: links to biodiversification?,

Edward, O., Korte, C., Ullmann, C. V., Colmenar, J., Thibault, N., Bagnoli, G., Stouge, S., and Rasmussen, C. M. Ø.: A Baltic Perspective on the Early to Early Late Ordovician δ13C and δ18O Records and Its Paleoenvironmental Significance, Paleoceanography and Paleoclimatology, 37, e2021PA004309, https://doi.org/10.1029/2021PA004309, 2022.

Edwards, C. T. and Saltzman, M. R.: Carbon isotope ($\delta^{13}C_{carb}$) stratigraphy of the Lower-Middle Ordovician (Tremadocian-Darriwilian) in the Great Basin, western United States: Implications for global correlation, Palaeogeography Palaeoclimatology Palaeoecology, 399, 1-20, 10.1016/j.palaeo.2014.02.005, 2014.

Edwards, C. T. and Saltzman, M. R.: Paired carbon isotopic analysis of Ordovician bulk carbonate ($\delta^{13}C_{carb}$) and organic matter ($\delta^{13}C_{org}$) spanning the Great Ordovician Biodiversification Event, Palaeogeography Palaeoclimatology Palaeoecology, 458, 102-117, 10.1016/j.palaeo.2015.08.005, 2016.

Edwards, C. T., Saltzman, M. R., Royer, D. L., and Fike, D. A.: Oxygenation as a driver of the Great Ordovician Biodiversification Event, Nature Geoscience, 10, 925–929, https://doi.org/10.1038/s41561-017-0006-3, 2017.

Edwards, C. T., Jones, C. M., Quinton, P. C., and Fike, D. A.: Oxygen isotope (δ18O) trends measured from Ordovician conodont apatite using secondary ion mass spectrometry (SIMS): Implications for paleo-thermometry studies, GSA Bulletin, 134, 261-274, 10.1130/B35891.1, 2021.

Edwards, C. T., Saltzman, M. R., Royer, D. L., and Fike, D. A.: Oxygenation as a driver of the Great Ordovician Biodiversification Event, Nature Geoscience, 10, 925–929, https://doi.org/10.1038/s41561-017-0006-3, 2017.

Elrick, M., Reardon, D., Labour, W., Martin, J., Desrochers, A., and Pope, M.: Orbital-scale climate change and glacioeustasy during the early Late Ordovician (pre-Hirnantian) determined from δ18O values in marine apatite, Geology, 41, 775-778, 10.1130/G34363.1, 2013.

Fairchild, I. J., Spencer, A. M., Ali, D. O., Anderson, R. P., Anderton, R., Boomer, I., Dove, D., Evans, J. D., Hambrey, M. J., Howe, J., Sawaki, Y., Shields, G. A., Skelton, A., Tucker, M. E., Wang, Z., and Zhou, Y.:

Tonian-Cryogenian boundary sections of Argyll, Scotland, Precambrian research, 319, 37-64, https://doi.org/10.1016/j.precamres.2017.09.020, 2018.

Fan, J. X., .Shen, S. Z., Erwin, D. H., Sadler, P. M., Macleod, N., Cheng, Q. M., Hou, X. D., Yang, J., Wang, X. D., Wang, Y., Zhang, H., Chen, X., Li, G. X., Zhang, Y. C., Shi, Y. K., Yuan, D. X., Chen, Q., Zhang, L. N., Li, C., and Zhao, Y. Y.: A high-resolution summary of Cambrian to early Triassic marine invertebrate biodiversity, Science, 367(6475): 272–277, https://doi.org/10.1126/science.aax4953, 2020.

Fan, R., Bergström, S. M., Lu, Y. Z., Zhang, X. L., Zhang, S. B., Li, X., and Deng, S. H.: Upper Ordovician carbon isotope chemostratigraphy on the Yangtze Platform, Southwestern China: Implications for the correlation of the Guttenberg (δ^{13}C excursion (GICE) and paleoceanic change, Palaeogeography Palaeoclimatology Palaeoecology, 433, 81-90, 10.1016/j.palaeo.2015.05.016, 2015.

Finnegan, S., Bergmann, K., Eiler, J. M., Jones, D. S., Fike, D. A., Eisenman, I., Hughes, N. C., Tripati, A. K., and Fischer, W. W.: The Magnitude and Duration of Late Ordovician–Early Silurian Glaciation, Science, 331, 903-906, doi:10.1126/science.1200803, 2011.

Frank, T. D., Lyons, T. W., and Lohmann, K. C.: Isotopic evidence for the paleoenvironmental evolution of the Mesoproterozoic Helena Formation, Belt Supergroup, Montana, USA, Geochimica et Cosmochimica Acta, 61, 5023-5041, https://doi.org/10.1016/S0016-7037(97)80341-9, 1997.

Garbelli, C., Angiolini, L., Jadoul, F., and Brand, U.: Micromorphology and differential preservation of Upper Permian brachiopod low-Mg calcite, Chemical Geology, 298-299, 1-10, https://doi.org/10.1016/j.chemgeo.2011.12.019, 2012.

Gilleaudeau, G. J., Sahoo, S. K., Kah, L. C., Henderson, M. A., and Kaufman, A. J.: Proterozoic carbonates of the Vindhyan Basin, India: Chemostratigraphy and diagenesis, Gondwana Research, 57, 10-25, https://doi.org/10.1016/j.gr.2018.01.003, 2018.

Goldberg, S. L., Present, T. M., Finnegan, S., and Bergmann, K. D.: A high-resolution record of early Paleozoic climate, Proceedings of the National Academy of Sciences, 118, e2013083118, doi:10.1073/pnas.2013083118, 2021.

Goldman, D., Sadler, P. M., Leslie, S. A., Melchin, M. J., Agterberg, F. P., and Gradstein, F. M.: Chapter 20 - The Ordovician Period, in: Geologic Time Scale 2020, edited by: Gradstein, F. M., Ogg, J. G., Schmitz, M. D., and Ogg, G. M., Elsevier, 631-694, https://doi.org/10.1016/B978-0-12-824360-2.00020-6, 2020.

Gong, F. Y., Joachimski, M. M., Yan, G. Z., Li, L. X., Wei, X., and Wu, R. C.: Middle to Late Ordovician carbon isotope chemostratigraphy of the Lower Yangtze Platform: Implications for global correlation, Geological Journal, 56, 2772-2784, 10.1002/gj.4068, 2021.

Gorokhov, I., Semikhatov, M. A., Baskakov, A. V., Kutyavin, E. P., Melnikov, N. N., Sochava, A. V., and Turchenko, T. L.: Sr isotopic composition in Riphean, Vendian, and Lower Cambrian carbonates from Siberia, Stratigraphy and Geological Correlation, 3, 1-28, 1995.

Gregg, J., Bish, D., Kaczmarek, S., and Machel, H.: Mineralogy, nucleation and growth of dolomite in the laboratory and sedimentary environment: A review, Sedimentology, 62, 10.1111/sed.12202, 2015.

Grossman, E. L. and Joachimski, M. M.: Chapter 10 - Oxygen Isotope Stratigraphy, in: Geologic Time Scale 2020, edited by: Gradstein, F. M., Ogg, J. G., Schmitz, M. D., and Ogg, G. M., Elsevier, 279-307, https://doi.org/10.1016/B978-0-12-824360-2.00010-3, 2020.

Harper, D. A. T., Hammarlund, E. U., and Rasmussen, C. M.: End Ordovician extinctions: A coincidence of causes, Gondwana Research, 25(4), 1294–1307, https://doi.org/10.1016/j.gr.2012.12.021, 2014.

Henderson, M. A., Serra, F., Feltes, N. A., Albanesi, G. L., and Kah, L. C.: Paired isotope records of carbonate and organic matter from the Middle Ordovician of Argentina: Intrabasinal variation and effects of the marine chemocline, Palaeogeography Palaeoclimatology Palaeoecology, 490, 107-130, 10.1016/j.palaeo.2017.10.018, 2018.

Herrmann, A. D., Macleod, K. G., and Leslie, S. A.: Did a volcanic mega-eruption cause global cooling during the Late Ordovician?, PALAIOS, 25, 831-836, 10.2110/palo. 2010.p10-069r, 2010.

Higgins, J. A., Blättler, C. L., Lundstrom, E. A., Santiago-Ramos, D. P., Akhtar, A. A., Crüger Ahm, A. S., Bialik, O., Holmden, C., Bradbury, H., Murray, S. T., and Swart, P. K.: Mineralogy, early marine diagenesis, and the chemistry of shallow-water carbonate sediments, Geochimica et Cosmochimica Acta, 220, 512-534, https://doi.org/10.1016/j.gca.2017.09.046, 2018.

Horacek, M., Povoden, E., Richoz, S., and Brandner, R.: High-resolution carbon isotope changes, litho- and magnetostratigraphy across Permian-Triassic Boundary sections in the Dolomites, N-Italy. New constraints for global correlation, Palaeogeography, Palaeoclimatology, Palaeoecology, 290, 58-64, https://doi.org/10.1016/j.palaeo.2010.01.007, 2010.

Hu, D. P., Zhang, X. L., Li, M. H., Xu, Y. L., and Shen, Y. N.: Carbon isotope ($\delta^{13}C_{carb}$) stratigraphy of the Lower-Upper Ordovician of the Yangtze Platform, South China: Implications for global correlation and the Great Ordovician Biodiversification Event (GOBE), Global and Planetary Change, 203, 10.1016/j.gloplacha.2021.103546, 2021.

Husinec, A. and Leslie, S. A.: Continuous record of Upper Ordovician (Katian) to lower Silurian (Telychian) global $\delta^{13}C$ excursions in the Williston Basin, Terra Nova, 34, 314-322, 10.1111/ter.12593, 2022.

Jacobsen, S. B. and Kaufman, A. J.: The Sr, C and O isotopic evolution of Neoproterozoic seawater, Chemical Geology, 161, 37-57, https://doi.org/10.1016/S0009-2541(99)00080-7, 1999.

Jiang, Q., Wu, J., Wang, H., Kuang, L., Zhou, Z., Yang, Y., Li, Y., Luo, C., Deng, B., and Jiao, K.: Thermal evolution of organic matter in the Lower Silurian Longmaxi Formation, southern Sichuan Basin and its main controlling factors, Oil & Gas Geology, 45, 1321-1336, 2024.

Jin, J., Zhan, R., and Wu, R.: Equatorial cold-water tongue in the Late Ordovician, Geology, 46, 759-762, 10.1130/G45302.1, 2018.

Joachimski, M. M., van Geldern, R., Breisig, S., Buggisch, W., and Day, J.: Oxygen isotope evolution of biogenic calcite and apatite during the Middle and Late Devonian, International Journal of Earth Sciences, 93, 542-553, 10.1007/s00531-004-0405-8, 2004.

Joachimski, M. M., Breisig, S., Buggisch, W., Talent, J. A., Mawson, R., Gereke, M., Morrow, J. R., Day, J., and Weddige, K.: Devonian climate and reef evolution: Insights from oxygen isotopes in apatite, Earth and Planetary Science Letters, 284, 599-609, https://doi.org/10.1016/j.epsl.2009.05.028, 2009.

Jones, D. S., Creel, R. C., and Rios, B. A.: Carbon isotope stratigraphy and correlation of depositional sequences in the Upper Ordovician Ely Springs Dolostone, eastern Great Basin, USA, Palaeogeography Palaeoclimatology Palaeoecology, 458, 85-101, 10.1016/j.palaeo.2016.01.036, 2016.

Jones, D. S., Fike, D. A., Finnegan, S., Fischer, W. W., Schrag, D. P., and McCay, D.: Terminal Ordovician carbon isotope stratigraphy and glacioeustatic sea-level change across Anticosti Island (Quebec, Canada), Geological Society of America Bulletin, 123, 1645-1664, 10.1130/b30323.1, 2011.

Jones, L. A. and Eichenseer, K.: Uneven spatial sampling distorts reconstructions of Phanerozoic seawater temperature, Geology, 50, 238-242, 10.1130/G49132.1, 2021.

Judd, E. J., Tierney, J. E., Huber, B. T., Wing, S. L., Lunt, D. J., Ford, H. L., Inglis, G. N., McClymont, E. L., O'Brien, C. L., Rattanasriampaipong, R., Si, W., Staitis, M. L., Thirumalai, K., Anagnostou, E., Cramwinckel, M. J., Dawson, R. R., Evans, D., Gray, W. R., Grossman, E. L., Henehan, M. J., Hupp, B. N., MacLeod, K. G., O'Connor, L. K., Sánchez Montes, M. L., Song, H., and Zhang, Y. G.: The PhanSST global database of Phanerozoic sea surface temperature proxy data, Scientific Data, 9, 753, 10.1038/s41597-022-01826-0, 2022.

Kah, L. C., Bartley, J. K., and Teal, D. A.: Chemostratigraphy of the Late Mesoproterozoic Atar Group, Taoudeni Basin, Mauritania: Muted isotopic variability, facies correlation, and global isotopic trends, Precambrian research, 200-203, 82-103, https://doi.org/10.1016/j.precamres.2012.01.011, 2012.

Kah, L. C., Sherman, A. G., Narbonne, G. M., Knoll, A. H., and Kaufman, A. J.: δ13C stratigraphy of the Proterozoic Bylot Supergroup, Baffin Island, Canada: implications for regional lithostratigraphic correlations, Canadian Journal of Earth Sciences, 36, 313-332, 10.1139/e98-100, 1999.

Kaljo, D., Martma, T., and Saadre, T.: Post-Hunnebergian Ordovician carbon isotope trend in Baltoscandia, its environmental implications and some similarities with that of Nevada, Palaeogeography Palaeoclimatology Palaeoecology, 245, 138-155, 10.1016/j.palaeo.2006.02.020, 2007.

Kaljo, D., Hints, L., Martma, T., Nolvak, J., and Oraspold, A.: Late Ordovician carbon isotope trend in Estonia, its significance in stratigraphy and environmental analysis, Palaeogeography Palaeoclimatology Palaeoecology, 210, 165-185, 10.1016/j.palaeo.2004.02.044, 2004.

Kaufman, A. J. and Knoll, A. H.: Neoproterozoic variations in the C-isotopic composition of seawater: stratigraphic and biogeochemical implications, Precambrian research, 73, 27-49, https://doi.org/10.1016/0301-9268(94)00070-8, 1995.

Kaufman, A. J., Hayes, J. M., Knoll, A. H., and Germs, G. J.: Isotopic compositions of carbonates and organic carbon from upper Proterozoic successions in Namibia: stratigraphic variation and the effects of diagenesis and metamorphism, Precambrian research, 49, 301-327, 10.1016/0301-9268(91)90039-d, 1991.

Kim, S.-T. and O'Neil, J. R.: Equilibrium and nonequilibrium oxygen isotope effects in synthetic carbonates, Geochimica et Cosmochimica Acta, 61, 3461-3475, https://doi.org/10.1016/S0016-7037(97)00169-5, 1997.

Knauth, L. P. and Kennedy, M. J.: The late Precambrian greening of the Earth, Nature, 460, 728-732, 10.1038/nature08213, 2009.

Kouchinsky, A., Bengtson, S., Gallet, Y., Korovnikov, I., Pavlov, V., Runnegar, B., Shields, G., Veizer, J., Young, E., and Ziegler, K.: The SPICE carbon isotope excursion in Siberia: a combined study of the upper Middle Cambrian-lowermost Ordovician Kulyumbe River section, northwestern Siberian Platform, Geological Magazine, 145, 609-622, 10.1017/s0016756808004913, 2008.

Kröger, B., Franeck, F., and Rasmussen, C. M.: The evolutionary dynamics of the early Palaeozoic marine biodiversity accumulation, Procee Proc Biol Sci, 286, 20191634, https://doi.org/10.1098/rspb.2019.1634, 2019.

Kump, L. R., Arthur, M. A., Patzkowsky, M. E., Gibbs, M. T., Pinkus, D. S., and Sheehan, P. M.: A weathering hypothesis for glaciation at high atmospheric pCO_2 during the Late Ordovician, Palaeogeography Palaeoclimatology Palaeoecology, 152, 173-187, 10.1016/s0031-0182(99)00046-2, 1999.

LaPorte, D. F., Holmden, C., Patterson, W. P., Loxton, J. D., Melchin, M. J., Mitchell, C. E., Finney, S. C., and Sheets, H. D.: Local and global perspectives on carbon and nitrogen cycling during the Hirnantian glaciation, Palaeogeography Palaeoclimatology Palaeoecology, 276, 182-195, 10.1016/j.palaeo.2009.03.009, 2009.

Lécuyer, C., Amiot, R., Touzeau, A., and Trotter, J.: Calibration of the phosphate $\delta^{18}O$ thermometer with carbonate–water oxygen isotope fractionation equations, Chemical Geology, 347, 217-226, https://doi.org/10.1016/j.chemgeo.2013.03.008, 2013.

Lindskog, A., Young, S. A., Bowman, C. N., Kozik, N. P., Newby, S. M., Eriksson, M. E., Pettersson, J., Molin, E., and Owens, J. D.: Oxygenation of the Baltoscandian shelf linked to Ordovician biodiversification, Nature Geoscience, 16, 1047–1053, 10.1038/s41561-023-01287-z, 2023.

Li, B. Y., Zhang, D. W., Pang, X. Q., Gao, P., Zhu, D. Y., Guo, K. Z., and Zheng, T. Y.: Paired $\delta^{13}C_{carb}$ and $\delta^{13}C_{org}$ records of the Ordovician on the Yangtze platform, South China, Australian Journal of Earth Sciences, 65, 809-822, 10.1080/08120099.2018.1487468, 2018.

Li, Y. X., Lin, J. H., Long, K. Y., Li, J. H. and Zhang, L. Y.: Gas potential of Lower Paleozoic marine mud-shale in the Middle Yangtze region, Geological Bulletin of China, 30, 349-356, 2011.

Liu, C. G., Li, G. R., Wang, D. W., Liu, Y. L., Luo, M. X., and Shao, X. M.: Middle Upper Ordovician (Darriwilian-Early Katian) Positive Carbon Isotope Excursions in the Northern Tarim Basin, Northwest

China: Implications for Stratigraphic Correlation and Paleoclimate, Journal of Earth Science, 27, 317-328, 10.1007/s12583-016-0696-2, 2016.

Liu, K., Jiang, M., Zhang, L., and Chen, D.: A new high-resolution palaeotemperature record during the Middle–Late Ordovician transition derived from conodont δ18O palaeothermometry, Journal of the Geological Society, 179, jgs2021-2148, 10.1144/jgs2021-148, 2022a.

Liu, M., Chen, D. Z., Jiang, L., Stockey, R. G., Aseal, D., Zhang, B., Liu, K., Yang, X. R., Yan, D. T., and Planavsky, N. J.: Oceanic anoxia and extinction in the latest Ordovician, Earth and Planetary Science Letters, 588, 10.1016/j.epsl.2022.117553, 2022b.

Liu, M., Bao, X., Harper, D. A. T., Algeo, T., Zhao, M., Saltzman, M., Zhang, W., Chen, D., Yuan, S., Chen, Y., Wei, M., Zhang, J., Luan, X., Zhang, Y., Yang, X., and Hu, Y.: Diversification to extinction: oceanic and climatic context of the Ordovician, Earth-Science Reviews, 269, 105194, https://doi.org/10.1016/j.earscirev.2025.105194, 2025.

Ma, X., Wang, Z. H., Zhang, Y. D., Song, Y. Y., and Fang, X.: Carbon isotope records of the Middle-Upper Ordovician transition in Yichang area, South China, Palaeoworld, 24, 136-148, 10.1016/j.palwor.2015.03.006, 2015.

Männik, P., Lehnert, O., Nõlvak, J., and Joachimski, M. M.: Climate changes in the pre-Hirnantian Late Ordovician based on $\delta^{18}O_{phos}$ studies from Estonia, Palaeogeography, Palaeoclimatology, Palaeoecology, 569, 110347, https://doi.org/10.1016/j.palaeo.2021.110347, 2021.

Marshall, J. D.: Climatic and oceanographic isotopic signals from the carbonate rock record and their preservation, Geological Magazine, 129, 143-160, 1992.

Mauviel, A., Sinnesael, M., and Desrochers, A.: The stratigraphic and geochemical imprints of Late Ordovician glaciation on far-field neritic carbonates, Anticosti Island, eastern Canada, Palaeogeography Palaeoclimatology Palaeoecology, 543, 10.1016/j.palaeo.2019.109579, 2020.

McArthur, J. M.: Recent trends in strontium isotope stratigraphy, Terra Nova, 6, 331-358, https://doi.org/10.1111/j.1365-3121.1994.tb00507.x, 1994.

McLaughlin, P. I., Emsbo, P., Desrochers, A., Bancroft, A., Brett, C. E., Riva, J. F., Premo, W., Neymark, L., Achab, A., Asselin, E., and Emmons, M. M.: Refining 2 km of Ordovician chronostratigraphy beneath Anticosti Island utilizing integrated chemostratigraphy, Canadian Journal of Earth Sciences, 53, 865-874, 10.1139/cjes-2015-0242, 2016.

Melim, L. A., Swart, P. K., and Eberli, G. P.: Mixing-Zone Diagenesis in the Subsurface of Florida and the Bahamas, Journal of Sedimentary Research, 74, 904-913, 10.1306/042904740904, 2004.

Bernasconi, S. M., Daëron, M., Bergmann, K. D., Bonifacie, M., Meckler, A. N., Affek, H. P., Anderson, N., Bajnai, D., Barkan, E., Beverly, E., Blamart, D., Burgener, L., Calmels, D., Chaduteau, C., Clog, M., Davidheiser-Kroll, B., Davies, A., Dux, F., Eiler, J., Elliott, B., Fetrow, A. C., Fiebig, J., Goldberg, S., Hermoso, M., Huntington, K. W., Hyland, E., Ingalls, M., Jaggi, M., John, C. M., Jost, A. B., Katz, S., Kelson, J., Kluge, T., Kocken, I. J., Laskar, A., Leutert, T. J., Liang, D., Lucarelli, J., Mackey, T. J., Mangenot, X., Meinicke, N., Modestou, S. E., Müller, I. A., Murray, S., Neary, A., Packard, N., Passey, B. H., Pelletier, E., Petersen, S., Piasecki, A., Schauer, A., Snell, K. E., Swart, P. K., Tripati, A., Upadhyay, D., Vennemann, T., Winkelstern, I., Yarian, D., Yoshida, N., Zhang, N., and Ziegler, M.: InterCarb: A community effort to improve interlaboratory standardization of the carbonate clumped isotope thermometer using carbonate standards, Geochem. Geophys. Geosyst., 22, e2020GC009588, https://doi.org/10.1029/2020GC009588, 2021.

Metzger, J. G. and Fike, D. A.: Techniques for assessing spatial heterogeneity of carbonate $\delta^{13}C$ values: Implications for craton-wide isotope gradients, Sedimentology, 60, 1405-1431, 10.1111/sed.12033, 2013.

Middleton, P. D., Marshall, J. D., and Brenchley, P. J.: Evidence for isotopic change associated with late ordovician glaciation from brachiopods and marine cements of central Sweden,

Montañez, I. P. and Crossey, L. J.: Diagenesis, in: Encyclopedia of Geochemistry: A Comprehensive Reference Source on the Chemistry of the Earth, edited by: White, W. M., Springer International Publishing, Cham, 353-362, 10.1007/978-3-319-39312-4_35, 2018.

Moore, C. H. and Wade, W. J.: Chapter 6 - Marine Diagenetic Environment, in: Developments in Sedimentology, edited by: Moore, C. H., and Wade, W. J., Elsevier, 93-131, https://doi.org/10.1016/B978-0-444-53831-4.00006-9, 2013a.

Moore, C. H. and Wade, W. J.: Chapter 5 - Carbonate Diagenesis: Introduction and Tools, in: Developments in Sedimentology, edited by: Moore, C. H., and Wade, W. J., Elsevier, 67-89, https://doi.org/10.1016/B978-0-444-53831-4.00005-7, 2013b.

Morse, J. W. and Mackenzie, F. T.: Chapter 3 Coprecipitation Reactions and Solid Solutions of Carbonate Minerals, in: Developments in Sedimentology, edited by: Morse, J. W., and Mackenzie, F. T., Elsevier, 87-132, https://doi.org/10.1016/S0070-4571(08)70332-7, 1990.

Munnecke, A., Zhang, Y. D., Liu, X., and Cheng, J. F.: Stable carbon isotope stratigraphy in the Ordovician of South China, Palaeogeography Palaeoclimatology Palaeoecology, 307, 17-43, 10.1016/j.palaeo.2011.04.015, 2011.

Ovchinnikova, G. V., Gorokhov, I. M., and Belyatskii, B. V.: U-Pb systematics of pre-Cambrian carbonates: The Riphean Sukhaya Tunguska Formation in the Turukhansk Uplift, Siberia, Lithology and Mineral Resources, 30, 1995.

Petrash, D. A., Bialik, O. M., Bontognali, T. R. R., Vasconcelos, C., Roberts, J. A., McKenzie, J. A., and Konhauser, K. O.: Microbially catalyzed dolomite formation: From near-surface to burial, Earth-Science Reviews, 171, 558-582, https://doi.org/10.1016/j.earscirev.2017.06.015, 2017.

Ping, Z.: Thermal Evolution and Effectivity of Source Rocks of the Lower-Paleozoic in Lower Yangtze Region, Natural Gas Geoscience, 21, 54-61, 2010.

Pohl, A., Wong Hearing, T. W., Brayard, A., Grossman, E., Joachimski, M. M., Le Hir, G., Letulle, T., Lunt, D. J., Martinez, M., Puceat, E., Suan, G., Valdes, P., and Donnadieu, Y.: Spatial biases in oxygen-based Phanerozoic seawater temperature reconstructions, Earth and Planetary Science Letters, 663, 119418, https://doi.org/10.1016/j.epsl.2025.119418, 2025.

Pucéat, E., Joachimski, M. M., Bouilloux, A., Monna, F., Bonin, A., Motreuil, S., Morinière, P., Hénard, S., Mourin, J., Dera, G., and Quesne, D.: Revised phosphate–water fractionation equation reassessing paleotemperatures derived from biogenic apatite, Earth and Planetary Science Letters, 298, 135-142, https://doi.org/10.1016/j.epsl.2010.07.034, 2010.

Pulsipher, M. A., Schiffbauer, J. D., Jeffrey, M. J., Huntley, J. W., Fike, D. A., and Shelton, K. L.: A meta-analysis of the Steptoean Positive Carbon Isotope Excursion: The SPICEraq database, Earth-Science Reviews, 212, 103442, https://doi.org/10.1016/j.earscirev.2020.103442, 2021.

Qing, H. and Veizer, J.: Oxygen and carbon isotopic composition of Ordovician brachiopods: Implications for coeval seawater, Geochimica et Cosmochimica Acta, 58, 4429-4442, https://doi.org/10.1016/0016-7037(94)90345-X, 1994.

Quinn, T. M.: Meteoric diagenesis of Plio-Pleistocene limestones at Enewetak Atoll, Journal of Sedimentary Research, 61, 681-703, 10.1306/D42677B2-2B26-11D7-8648000102C1865D, 1991.

Quinton, P. C. and MacLeod, K. G.: Oxygen isotopes from conodont apatite of the midcontinent, US: Implications for Late Ordovician climate evolution, Palaeogeography, Palaeoclimatology, Palaeoecology, 404, 57-66, https://doi.org/10.1016/j.palaeo.2014.03.036, 2014.

Quinton, P. C., Rygel, M. C., and Heins, M.: Sequence stratigraphy and carbon isotopes from the Trenton and Black River Groups near Union Furnace, PA: Constraining the role of land plants in the Ordovician world, Palaeogeography Palaeoclimatology Palaeoecology, 574, 10.1016/j.palaeo.2021.110440, 2021.

Quinton, P. C., Herrmann, A. D., Leslie, S. A., and MacLeod, K. G.: Carbon cycling across the southern margin of Laurentia during the Late Ordovician, Palaeogeography Palaeoclimatology Palaeoecology, 458, 63-76, 10.1016/j.palaeo.2015.08.020, 2016.

Quinton, P. C., Speir, L., Miller, J., Ethington, R., and Macleod, K. G.: Extreme heat in the Early Ordovician, PALAIOS, 33, 353-360, 10.2110/palo. 2018.031, 2018.

Quinton, P. C., Law, S., Macleod, K. G., Herrmann, A. D., Haynes, J. T., and Leslie, S. A.: Testing the early Late Ordovician cool-water hypothesis with oxygen isotopes from conodont apatite, Geological Magazine, 155, 1727-1741, 10.1017/S0016756817000589, 2017.

Rasmussen, C. M. Ø., Ullmann, C. V., Jakobsen, K. G., Lindskog, A., Hansen, J., Hansen, T., Eriksson, M. E., Dronov, A., Frei, R., Korte, C., Nielsen, A. T., and Harper, D. A. T.: Onset of main Phanerozoic marine radiation sparked by emerging Mid Ordovician icehouse, Scientific Reports, 6, 18884, 10.1038/srep18884, 2016.

Rimstidt, J. D., Balog, A., and Webb, J.: Distribution of trace elements between carbonate minerals and aqueous solutions, Geochimica et Cosmochimica Acta, 62, 1851-1863, https://doi.org/10.1016/S0016-7037(98)00125-2, 1998.

Rosenau, N. A., Herrmann, A. D., and Leslie, S. A.: Conodont apatite δ18O values from a platform margin setting, Oklahoma, USA: Implications for initiation of Late Ordovician icehouse conditions, Palaeogeography, Palaeoclimatology, Palaeoecology, 315-316, 172-180, https://doi.org/10.1016/j.palaeo.2011.12.003, 2012.

Rohatgi, A.: WebPlotDigitizer, Version 4.5, https://github.com/automeris-io/WebPlotDigitizer/releases/tag/v4.5 (last access: 30 August 2026), 2021.

Rubinson, M. and Clayton, R. N.: Carbon-13 fractionation between aragonite and calcite, Geochimica et Cosmochimica Acta, 33, 997-1002, https://doi.org/10.1016/0016-7037(69)90109-4, 1969.

Saltzman, M. R.: Late Paleozoic ice age: Oceanic gateway or pCO2?, Geology, 31, 151-154, 10.1130/0091-7613(2003)031<0151:LPIAOG>2.0.CO;2, 2003.

Saltzman, M. R.: Phosphorus, nitrogen, and the redox evolution of the Paleozoic oceans, Geology, 33, 573-576, 10.1130/G21535.1, 2005.

Saltzman, M. R. and Young, S. A.: Long-lived glaciation in the Late Ordovician? Isotopic and sequence-stratigraphic evidence from western Laurentia, Geology, 33, 109-112, 10.1130/g21219.1, 2005.

Sandberg, P. A.: An oscillating trend in Phanerozoic non-skeletal carbonate mineralogy, Nature, 305, 19-22, 10.1038/305019a0, 1983.

Sepkoski, J. J.: The Ordovician Radiations: Diversification and Extinction Shown by Global Genus-Level Taxonomic Data, In: Cooper C, Droser M, Finney S. (Eds.). 7th International Symposium on the Ordovician System, Las Vegas: SEPM Publication, 77, 75–80, 1995.

Servais, T., Harper, D., Munnecke, A., Owen, A., and Sheehan, P.: Understanding the Great Ordovician Biodiversification Event (GOBE): Influences of paleogeography, paleoclimate, or paleoecology?, GSA Today, 19, 4–10, 10.1130/GSATG37A.1, 2009.

Servais, T., Perrier, V., Danelian, T., Klug, C., Martin, R., Munnecke, A., Nowak, H., Nützel, A., Vandenbroucke, T. R., Williams, M., and Rasmussen, C. M.: The onset of the 'Ordovician Plankton Revolution' in the late Cambrian, Palaeogeography, Palaeoclimatology, Palaeoecology, 458, 12-28, https://doi.org/10.1016/j.palaeo.2015.11.003, 2016.

Sheehan, P. M.: The Late Ordovician Mass Extinction, Annual Review of Earth and Planetary Sciences, 29, 331-364, https://doi.org/10.1146/annurev.earth.29.1.331, 2001.

Shields, G. and Veizer, J.: Precambrian marine carbonate isotope database: Version 1.1, Geochemistry, Geophysics, Geosystems, 3, 1 of 12-12 of 12, https://doi.org/10.1029/2001GC000266, 2002.

Shields, G. A., Carden, G. A. F., Veizer, J., Meidla, T., Rong, J.-Y., and Li, R.-Y.: Sr, C, and O isotope geochemistry of Ordovician brachiopods: a major isotopic event around the Middle-Late Ordovician transition, Geochimica et Cosmochimica Acta, 67, 2005-2025, https://doi.org/10.1016/S0016-7037(02)01116-X, 2003.

Sial, A. N., Peralta, S., Gaucher, C., Toselli, A. J., Ferreira, V. P., Frei, R., Parada, M. A., Pimentel, M. M., and Pereira, N. S.: High-resolution stable isotope stratigraphy of the upper Cambrian and Ordovician in the Argentine Precordillera: Carbon isotope excursions and correlations, Gondwana Research, 24, 330-348, 10.1016/j.gr.2012.10.014, 2013.

Stanley, S. M.: Estimates of the magnitudes of major marine mass extinctions in earth history, Proceedings of the National Academy of Sciences, 113, E6325–E6334, https://doi.org/10.1073/pnas.1613094113, 2016.

Swart, P. K.: The geochemistry of carbonate diagenesis: The past, present and future, Sedimentology, 62, 1233-1304, 10.1111/sed.12205, 2015.

Sweet, W. C., 1989. The Conodonta: Morphology, Taxonomy, Paleoecology, and Evolutionary History of a Long - Extinct Animal Phylum. Oxford University Press, Oxford.

Thiagarajan, N., Lepland, A., Ryb, U., Torsvik, T. H., Ainsaar, L., Hints, O., and Eiler, J.: Reconstruction of Phanerozoic climate using carbonate clumped isotopes and implications for the oxygen isotopic composition of seawater, Proceedings of the National Academy of Sciences of the United States of America, 121, e2400434121, 10.1073/pnas.2400434121, 2024.

Thompson, C. K. and Kah, L. C.: Sulfur isotope evidence for widespread euxinia and a fluctuating oxycline in Early to Middle Ordovician greenhouse oceans, Palaeogeography Palaeoclimatology Palaeoecology, 313, 189-214, 10.1016/j.palaeo.2011.10.020, 2012.

Trela, W., Krzeminska, E., Jewula, K., and Czupyt, Z.: Oxygen Isotopes from Apatite of Middle and Late Ordovician Conodonts in Peri-Baltica (The Holy Cross Mountains, Poland) and Their Climatic Implications, Geosciences, 12, 10.3390/geosciences12040165, 2022.

Trotter, J. A., Williams, I. S., Barnes, C. R., Lécuyer, C., and Nicoll, R. S.: Did Cooling Oceans Trigger Ordovician Biodiversification? Evidence from Conodont Thermometry, Science, 321, 550-554, doi:10.1126/science. 1155814, 2008.

Trotter, J. A., Williams, I. S., Barnes, C. R., Männik, P., and Simpson, A.: New conodont δ18O records of Silurian climate change: Implications for environmental and biological events, Palaeogeography, Palaeoclimatology, Palaeoecology, 443, 34-48, https://doi.org/10.1016/j.palaeo.2015.11.011, 2016.

Trotter, J. A., Williams, I. S., Nicora, A., Mazza, M., and Rigo, M.: Long-term cycles of Triassic climate change: a new $\delta^{18}O$ record from conodont apatite, Earth and Planetary Science Letters, 415, 165-174, https://doi.org/10.1016/j.epsl.2015.01.038, 2015.

Veizer, J.: Chemical Diagenesis of Carbonates: Theory and Application of Trace Element Technique, 10.2110/scn.83.01.0000, 1983.

Veizer, J., Clayton, R. N., and Hinton, R. W.: Geochemistry of Precambrian carbonates: IV. Early Paleoproterozoic (2.25 ± 0.25 ga) seawater, Geochimica et Cosmochimica Acta, 56, 875-885, https://doi.org/10.1016/0016-7037(92)90033-F, 1992a.

Veizer, J., Fritz, P., and Jones, B.: Geochemistry of brachiopods: Oxygen and carbon isotopic records of Paleozoic oceans, Geochimica et Cosmochimica Acta, 50, 1679-1696, https://doi.org/10.1016/0016-7037(86)90130-4, 1986.

Veizer, J., Plumb, K. A., Clayton, R. N., Hinton, R. W., and Grotzinger, J. P.: Geochemistry of Precambrian carbonates: V. Late Paleoproterozoic seawater, Geochimica et Cosmochimica Acta, 56, 2487-2501, https://doi.org/10.1016/0016-7037(92)90204-V, 1992b.

Veizer, J., Ala, D., Azmy, K., Bruckschen, P., Buhl, D., Bruhn, F., Carden, G. A. F., Diener, A., Ebneth, S., Godderis, Y., Jasper, T., Korte, C., Pawellek, F., Podlaha, O. G., and Strauss, H.: $^{87}Sr/^{86}Sr$, $\delta^{13}C$ and $\delta^{18}O$ evolution of Phanerozoic seawater, Chemical Geology, 161, 59-88, https://doi.org/10.1016/S0009-2541(99)00081-9, 1999.

Wadleigh, M. A. and Veizer, J.: 18O16O and 13C12C in lower Paleozoic articulate brachiopods: Implications for the isotopic composition of seawater, Geochimica et Cosmochimica Acta, 56, 431-443, https://doi.org/10.1016/0016-7037(92)90143-7, 1992.

Warren, J.: Dolomite: occurrence, evolution and economically important associations, Earth-Science Reviews, 52, 1-81, https://doi.org/10.1016/S0012-8252(00)00022-2, 2000.

Westerhold, T., Marwan, N., Drury, A. J., Liebrand, D., Agnini, C., Anagnostou, E., Barnet, J. S. K., Bohaty, S. M., De Vleeschouwer, D., Florindo, F., Frederichs, T., Hodell, D. A., Holbourn, A. E., Kroon, D., Lauretano, V., Littler, K., Lourens, L. J., Lyle, M., Pälike, H., Röhl, U., Tian, J., Wilkens, R. H., Wilson, P. A., and Zachos, J. C.: An astronomically dated record of Earth's climate and its predictability over the last 66 million years, Science, 369, 1383-1387, 10.1126/science.aba6853, 2020.

Wheeley, J. R., Smith, M. P., and Boomer, I.: Oxygen isotope variability in conodonts: implications for reconstructing Palaeozoic palaeoclimates and palaeoceanography, Journal of the Geological Society, 169, 239-250, 10.1144/0016-76492011-048, 2012.

Wheeley, J. R., Jardine, P. E., Raine, R. J., Boomer, I., and Smith, M. P.: Paleoecologic and paleoceanographic interpretation of δ18O variability in Lower Ordovician conodont species, Geology, 46, 467-470, 10.1130/G40145.1, 2018.

Wu, R. C., Calner, M., and Lehnert, O.: Integrated conodont biostratigraphy and carbon isotope chemostratigraphy in the Lower-Middle Ordovician of southern Sweden reveals a complete record of the MDICE, Geological Magazine, 154, 334-353, 10.1017/s0016756816000017, 2017.

Wu, R. C., Calner, M., Lehnert, O., Lindskog, A., and Joachimski, M.: Conodont biostratigraphy and carbon isotope stratigraphy of the Middle Ordovician (Darriwilian) Komstad Limestone, southern Sweden, Journal of the Geological Society, 140, 44-54, 10.1080/11035897.2018.1435561, 2018.

Wu, R. C., Liu, J. B., Calner, M., Gong, F. Y., Lehnert, O., Luan, X. C., Li, L. X., and Zhan, R. B.: High-resolution carbon isotope stratigraphy of the Lower and Middle Ordovician succession of the Yangtze Platform, China: implications for global correlation, Journal of the Geological Society, 177, 537-549, 10.1144/jgs2018-208, 2020.

Xie, H., Zhao, J., Wang, P., Xie, W., and Yang, Y.: Ordovician sequence stratigraphic framework in the Middle-Upper Yangtze area, Acta Petrolei Sinica, 40, 1202-1222, 10.7623/syxb20191006, 2019.

Yang, X. Q., Li, Z., Fan, T. L., Gao, Z. Q., and Tang, S.: Carbon isotope ($\delta^{13}C_{carb}$) stratigraphy of the Early-Middle Ordovician (Tremadocian-Darriwilian) carbonate platform in the Tarim Basin, NW China: implications for global correlations, Geological Magazine, 158, 487-508, 10.1017/s0016756820000643, 2021.

Yang, F. Z., Yan, J. Z., Su, S. A., Yang, C. L., Huang, M., Guo, N. F., Wang, W. Y.: Evolution of marine basins in the Lower Yangtze region and assessment of exploration target areas for oil and gas, Jiangsu Geology, 134-141, 2001.

Young, S. A., Saltzman, M. R., and Bergström, S. M.: Upper Ordovician (Mohawkian) carbon isotope ($\delta^{13}C$) stratigraphy in eastern and central North America: Regional expression of a perturbation of the global carbon cycle, Palaeogeography Palaeoclimatology Palaeoecology, 222, 53-76, 10.1016/j.palaeo.2005.03.008, 2005.

Young, S. A., Gill, B. C., Edwards, C. T., Saltzman, M. R., and Leslie, S. A.: Middle-Late Ordovician (Darriwilian-Sandbian) decoupling of global sulfur and carbon cycles: Isotopic evidence from eastern and southern Laurentia, Palaeogeography Palaeoclimatology Palaeoecology, 458, 118-132, 10.1016/j.palaeo.2015.09.040, 2016.

Yin, Y. L.: Shale gas potential of the Lower Paleozoic shale strata in the Lower Yangtze, Unconventional Oil & Gas, 6, 26-32, 2019.

Young, S. A., Saltzman, M. R., Ausich, W. I., Desrochers, A., and Kaljo, D.: Did changes in atmospheric CO_2 coincide with latest Ordovician glacial-interglacial cycles?, Palaeogeography Palaeoclimatology Palaeoecology, 296, 376-388, 10.1016/j.palaeo.2010.02.033, 2010.

Yu, S. Y., Fang, X., Munnecke, A., Li, W. J., Zhen, Y. Y., Li, Y., Wang, Z. H., and Zhang, Y. D.: First documentation of Middle Ordovician warm-water carbonates in the Mount Jolmo Lungma (Mount Everest) area, southern Xizang (Tibet), China, and its paleogeographic implications, Palaeogeography Palaeoclimatology Palaeoecology, 530, 136-151, 10.1016/j.palaeo.2019.05.030, 2019.

ZAitsev, A. V. and Pokrovsky, B. G.: Carbon and oxygen isotope compositions of Lower-Middle Ordovician carbonate rocks in the northwestern Russian platform, Lithology and Mineral Resources, 49, 272-279, 10.1134/s0024490214030079, 2014.

Zhao, T. and Duan, H. L.: Shale gas formation condition of lower Paleozoic in the northern of Lower Yangtze, Complex Hydrocarbon Reservoirs, 12, 11-16+27, 10.16181/j.cnki.fzyqc.2019.01.003, 2019.

Zhang, T. G., Shen, Y. A., and Algeo, T. J.: High-resolution carbon isotopic records from the Ordovician of South China: Links to climatic cooling and the Great Ordovician Biodiversification Event (GOBE), Palaeogeography Palaeoclimatology Palaeoecology, 289, 102-112, 10.1016/j.palaeo.2010.02.020, 2010.

Zhang, Y. D. and Munnecke, A.: Ordovician stable carbon isotope stratigraphy in the Tarim Basin, NW China, Palaeogeography Palaeoclimatology Palaeoecology, 458, 154-175, 10.1016/j.palaeo.2015.09.001, 2016.

Zhao, H., Zhang, L., Algeo, T. J., Lyu, Z., Wang, X., and Hao, F.: Volcanism and basalt weathering drove Ordovician climatic cooling, Nature Communications, 16, 11475, 10.1038/s41467-025-66316-4, 2025.

Zhang, Z., Yang, C., Sahy, D., Zhan, R. B., Wu, R. C., Li, Y., Deng, Y., Huang, B., Condon, D. J., Rong, J., and Li, X. H.: Tempo of the Late Ordovician mass extinction controlled by the rate of climate change, Science advances, 11, eadv6788, 10.1126/sciadv.adv6788, 2025.

Zhang, Z., Wu, R., Lehnert, O., Calner, M., Rasmussen, C. M. Ø., Tang, G.-Q., and Li, X.-H.: Oxygen isotope-based evidence for stepwise climate cooling aligns with the tripartite division of the Ordovician, Global and Planetary Change, 257, 105246, https://doi.org/10.1016/j.gloplacha.2025.105246, 2026.